

Tobiasz Mazan

Multiscale Modeling of the Polyamide 11 Hydrolytic Degradation for Offshore Industry Applications

Comparison between model predictions and
experimental aging

Thesis for the Degree of Philosophiae Doctor

Trondheim, December 2015

Norwegian University of Science and Technology
Faculty of Engineering Science and Technology
Department of Engineering Design and Materials



NTNU
Norwegian University of Science and Technology

Thesis for the Degree of Philosophiae Doctor

Faculty of Engineering Science and Technology
Department of Engineering Design and Materials

© Tobiasz Mazan

ISBN 978-82-326-1316-8 (printed ver.)
ISBN 978-82-326-1317-5 (electronic ver.)
ISSN 1503-8181

Doctoral theses at NTNU, 2015:330

Printed by NTNU Grafisk senter

Maximillian Cohen, character from Pi (1998):

“11:15, restate my assumptions:

1. Mathematics is the language of nature.
2. Everything around us can be represented and understood through numbers.
3. If you graph these numbers, patterns emerge.

Therefore: There are patterns everywhere in nature”

ACKNOWLEDGEMENTS

First of all, thank you must go to Professor Andreas Echtermeyer for his belief in my ability and the project. Additionally, I would like to thank Dr. Jens Kjær Jørgensen and Dr. Terje Tofteberg, who were my co-supervisors throughout the duration of this doctoral study.

Many thanks to Randi Berggren, Britt Sommer and Huiting Jin, whose work contributed to much of the experimental results reported in this thesis. Honorary mention goes to Professor Rune Nydal, for the individual course, which was a highlight of my organized PhD training.

I would like to express my gratitude for the financial support by the Research Council of Norway (grant 193167).

Finally, I'm grateful to my friends from Warsaw, who did not forget about me after I moved abroad, to those I met during my time in Oslo and to my family, which provides one solid foundation in the ever-changing reality.

ABSTRACT

Hydrolytic degradation at elevated temperatures is a key reason for failure in offshore flexible risers. Polyamide 11 (PA11) is one of the most common materials used for the internal pressure sheaths in flexible risers due to good fatigue and creep resistance as well as decent barrier properties towards oil and natural gas. In the experimental part of this thesis the ageing of polyamide 11 in deoxygenated water at 90°C and 120°C was studied. Tensile and DMTA tests were performed to measure changes in mechanical properties. Viscometry, gravimetric measurements, DSC and TGA were used to link these properties with morphological changes.

Accelerated aging tests, followed by the Arrhenius based extrapolation, are the conventional way to evaluate long-term degradation of polymers, in particular for offshore flexible risers. In the theoretical part of this thesis a multiscale model has been developed combining diffusion, chemical kinetic reactions, structure-property relationships and composite models to provide faster and less labor extensive property predictions. A general methodology was presented and applied to predict morphology evolution and mechanical properties during the hydrolytic degradation of PA11. Results for density, degree of crystallinity, elastic modulus, tensile strength and embrittlement threshold have been compared with experimental aging in deoxygenated water at 120°C.

General trends observed in the experimental study were increased stiffness, tensile strength and glass transition temperature as well as decreased glassy state damping efficiency with increased ageing times. Changes can be initially ascribed to plasticizer depletion and then to interplay between molecular weight decrease and crystallinity increase. Viscosity at hydrolysis equilibrium indicated that brittle failure typically involves oxidation or UV exposure.

For both density and degree of crystallinity the modeled trend was close to the experimental test results. Accurate prediction of the morphological parameters during degradation allowed extension of the multiscale model for the prediction of mechanical properties. Similarly, in the case of mechanical properties the model correctly predicted the experimental test results confirming hydrolysis induced chain scission and chemicrystallisation as the two main mechanisms of property change. This suggests that the multiscale modeling methodology can provide a valuable alternative to accelerated aging tests. The model also indicated that the crystalline phase does play a role in the plastic deformation as opposed to the view that this is solely a matter of the amorphous phase. Moreover, the mechanical equilibrium between effects of macromolecule degradation and an increased degree of crystallinity has been described.

This work is structured as an article-based thesis. The papers that constitute the main part of this thesis are given in Part II. Part I places the included articles into a wider context and provides their summary.

LIST OF PAPERS

This thesis includes the following papers, referred to by capital letters in the text:

- A** Tobiasz Mazan, Randi Berggren, Jens Kjær Jørgensen and Andreas Echtermeyer
Aging of Polyamide 11. Part 1: Evaluating degradation by Thermal, Mechanical and Viscometric Analysis
Journal of Applied Polymer Science, vol. 132, no. 20, pp. 6249-6260; Feb 19, 2015
- B** Tobiasz Mazan, Jens Kjær Jørgensen and Andreas Echtermeyer
Aging of Polyamide 11. Part 2: General multiscale model of the hydrolytic degradation applied to predict the morphology evolution
Journal of Applied Polymer Science, vol. 132, no. 41, pp. 12039-12049; Aug 4, 2015
- C** Tobiasz Mazan, Jens Kjær Jørgensen and Andreas Echtermeyer
Aging of Polyamide 11. Part 3: Multiscale model predicting the mechanical properties after hydrolytic degradation
Journal of Applied Polymer Science, vol. 132, no. 46, pp. 13299-13310; Sep 8, 2015

TABLE OF CONTENTS

Acknowledgements	iv
Abstract.....	v
List of papers.....	vi
PART I INTRODUCTION	3
1. Outline of study	4
1.1. Motivation.....	4
1.2. Objectives	4
1.3. Research methods.....	5
1.4. Outcomes	5
2. Theoretical background	7
2.1. Flexible riser	7
2.2. Polyamide 11.....	8
2.3. Hydrolysis	9
2.4. Empirical service-life prediction.....	10
2.5. Multiscale modeling	12
3. Experimental techniques and materials	15
3.1. Material.....	15
3.2. Accelerated aging.....	15
3.3. Gravimetric measurements	16
3.4. Volatile extraction	16
3.5. Viscometric analysis.....	16
3.6. Differential Scanning Calorimetry (DSC)	17
3.7. Tensile test	17
3.8. Dynamic Mechanical Thermal Analysis (DMTA).....	18
4. Multiscale model of PA11 degradation	19
4.1. General description.....	19
4.2. Discussion.....	22
5. Summary of papers	24

6. Concluding remarks.....	27
6.1. Future work.....	27
7. References.....	29
 PART II INCLUDED PAPERS.....	 31
PAPER A.....	32
PAPER B	44
PAPER C	55

PART I

INTRODUCTION

1. Outline of Study

This chapter presents the motivation behind this PhD project, objectives set up in the research plan, methods used to realize them and the final outcomes the study brought to the scientific knowledge and engineering practice.

1.1. Motivation

Polyamide 11 (PA11) is commonly used as a material for the internal pressure sheaths in offshore flexible risers (**API**, 2003). It possesses good mechanical and barrier properties, however is also known to undergo chemical degradation once exposed to oil field exploration environments, especially water (**Arkema**, 2012).

Therefore, long term performance of the riser under chemical and mechanical factors must be evaluated. As of today, long term performance is evaluated by simple extrapolation of the experimental data for certain material (here PA11) in the expected environment to lifetimes up to 50 years. No consideration is given to the actual mechanisms behind the degradation process (**Flynn**, 1995).

Despite extensive laboratory testing; which requires labor, time and resources; actual failure in the field often happens long before (or after) the expected one (**4Subsea AS**, 2013). Also, without scientific understanding of the processes on the microscale, extrapolation of the results to different application cases is very difficult. In order to improve cost, accuracy and generality of predictions a general model of degradation is proposed here.

1.2. Objectives

The main objectives of this PhD study have been listed below:

- Develop a general methodology for lifetime prediction of polymers under environmental impact, which would:
 - Bring insight beyond the common Arrhenius based extrapolation,
 - Utilize diffusion and degradation mechanism on a micro level and use equations for degradation kinetics in global models for lifetime prediction,
 - Result in faster life-time prediction, requiring less testing,
 - Give good accuracy for the chosen model systems.
- Perform experiments on PA11 degradation (mostly due to hydrolysis) in water
- Adjust the general methodology based on the experimental results obtained for PA11

1.3. Research methods

A careful literature review was of key importance to find structure-properties databases and to use the right chemical degradation models. Models operating on different scale-levels have been chosen for their demonstrated accuracy and ability to fit the multiscale model in a relatively straightforward manner- avoiding major scale bridging issues.

Moreover, considerable usage of computer aided materials engineering was required. In general case the multiscale model developed here should be implemented in Matlab or equivalent environment. However, in the case of PA11 exposed to water diffusion proceeds very fast (**Wu & Siesler**, 2003) and the environmental agent can be considered uniformly distributed within the material. Therefore diffusion modeling is not necessary and the model becomes particularly simple to use due to the analytic form of its remaining expressions. Accurate predictions of polymer properties can be easily obtained with simple calculation spreadsheets, such as EXCEL, as long as degradation is not diffusion controlled.

In order to test the multiscale model predictions, the aging process of PA11 was examined by tracking the changes in mechanical and morphological properties. Accelerated aging was performed in deoxygenated water, since the internal pressure sheath PA11 in operative risers is exposed to an oxygen free environment (**Jacques**, et al., 2002). The mechanical test methods in question were Tensile Testing and Dynamic Mechanical Thermal Analysis (DMTA). The latter was performed to follow changes in the glass transition temperature and storage modulus. Weight measurements were performed to keep track on sample density and weight loss. Thermal Gravimetric Analysis investigated plasticizer extraction and Differential Scanning Calorimetry (DSC) crystallinity evolution.

In the early phases of the research work Molecular Modeling tools (LAMMPS, Ovito, Avogadro) were also used, however the topological method by (**Bicerano**, 2002) was chosen to be included into the final model instead. Additionally, the Finite Element Method codes (Abaqus, Ansys) may be utilized to supplement the multiscale approach described here.

1.4. Outcomes

The objectives of this doctoral study have been successfully realized. The aging process of PA11 in water has been studied in detail and the results have been published (*Paper A*). Similarly, the general multiscale methodology of the polymer degradation has been developed (*Paper B*) and applied to predict the morphological parameters (*Paper B*) and the mechanical properties (*Paper C*) during hydrolytic aging of PA11.

The project provided a unique way to improve polymer life-time prediction methodology by taking micro-scale mechanisms into account. The body of work included investigations on polymers applicable in offshore industry, mainly for flexible risers and sealing (namely PA 11). The most significant degradation mechanisms were identified among the many possible ones. The proposed methodology provided life-time predictions beyond the common Arrhenius based extrapolation. Local models on micro degradation and global models combining local effects were developed. The results suggest that the multiscale modeling methodology can provide faster and less labor extensive alternatives for accelerated aging tests when it comes to long-term property evaluation.

The analytic tool developed here could decrease economic loss due to unexpected failure of flexible risers and ecological hazards due to subsequent spill out of crude oil. Reliable tools for degradation prediction should also significantly speed up developments in plastics industry.

2. Theoretical Background

The following section provides the theoretical background required to fully understand the scientific articles included in Part II of this thesis.

2.1. Flexible riser

Oilfield flexible risers convey high temperature production fluids (typically mixtures of oil, gas and water) from subsea units on the seabed to topside platforms. The risers are multilayered pipes of metal and polymers designed to have high axial stiffness and rather low bending stiffness. They have an internal polymer sheath to keep the transported fluid inside the pipe. Unbonded metal strips are wound around this sheath to provide strength and stiffness. An outer thermoplastic sheath is a barrier against seawater ingress. An example of the flexible riser configuration is given in Figure 1. More details can be found in (API, 2008).

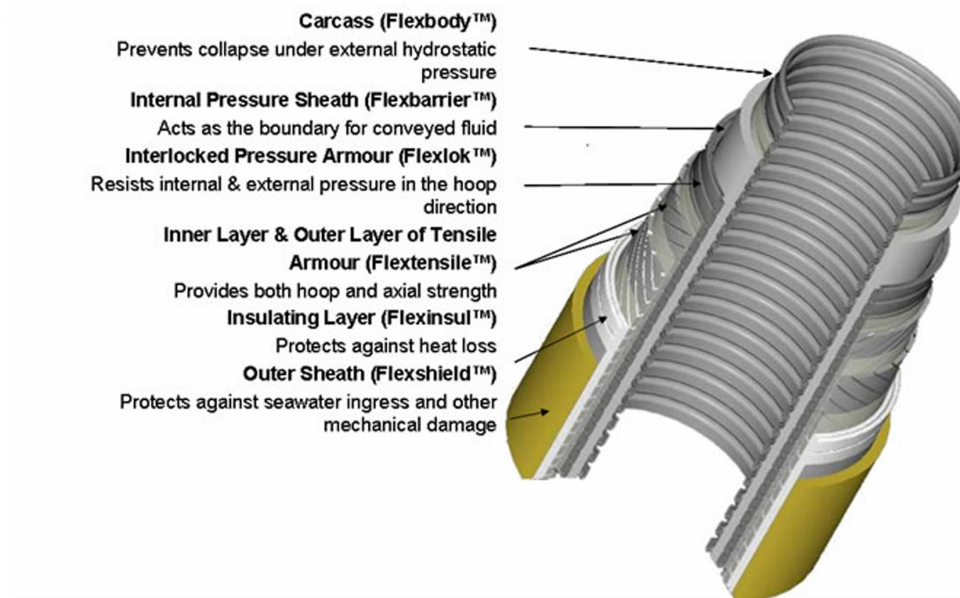


Figure 1. Basic layer configuration of a flexible riser. (**FlexiRiserTest**, 2010)

Flexible risers are of key importance for floating production units as they follow motions of the unit. In this case, dynamic motions of ships and semisubmersibles would likely cause failure of rigid risers. The same construction as used for flexible risers can also be used as pipelines.

Flexible pipelines tend to severely reduce the total installation cost compared to rigid pipeline installation (Simonsen, 2014). Rigid pipeline requires either significant seabed preparation for rough surfaces or typically longer (and more costly) pipelines as an alternative. Moreover, flexible pipes are largely immune to changes of the seabed structure over time.

The offshore environment presents many structural challenges to the flexible risers, such as the fluctuating dynamic loads imposed by surface waves and underwater currents. The polymer sheaths provide fluid tightness, they do not provide any structural strength, but they need to follow all deformations of the structure over its entire life. This means they need to have a fairly high strain to failure (a few %) and good fracture toughness. Strength and stiffness of the polymer sheath are needed to bridge the gaps between the metal parts and to prevent excessive creep into the gaps.

2.2. Polyamide 11

Polyamide 11 (PA11) is one of the most common materials used for the internal pressure sheaths in flexible risers due to good fatigue and creep resistance as well as high barrier properties towards oil and natural gas (**Arkema**, 2012). Based on literature, chiefly (**Berggren**, 2013), key information about microstructure and properties of PA11 is given below.

Polyamides (nylons) are the thermoplastic polymers characterized by the presence of the amide group in the backbone chain. Nomenclature of linear polyamides is based on the number of carbon atoms in the monomer. Therefore, PA11 has a total of eleven carbon atoms in each repeating unit as illustrated in Figure 2.

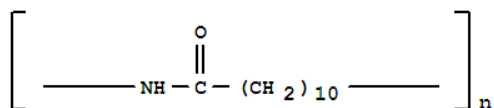


Figure 2. Molecular structure of the Polyamide 11 repeat unit. (**LookChem**, 2008)

The structure of the amide group is featured in Figure 3.

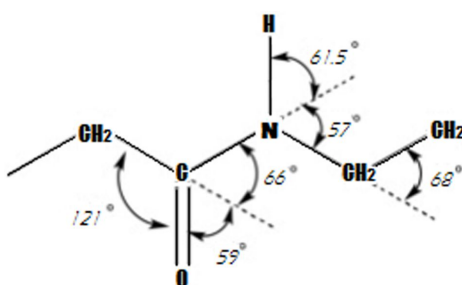


Figure 3. Conformation of the amide group in aliphatic nylons.

Polyamide 11 is a semicrystalline polymer with crystallites tied together by the amorphous regions. The crystalline phase is characterized by the long-range lattice orders, opposite to the amorphous phase, which merely exhibits short-range order. Molecules organized in the long-range order fold and assemble into thin crystals called lamellae. Then these crystalline lamellae stack together with amorphous layers forming spherically shaped aggregates termed spherulites (**Kohan**, 1995).

The crystal structure of PA11 has been extensively studied. PA properties strongly depend on hydrogen bonds formed between individual polymer chains. Hydrogen bonds can be considered the main energetic driver for the crystal forms of polyamides. PA11 is known to have at least 5 different crystal forms: a triclinic α -form, a monoclinic β form and three hexagonal forms (γ , δ and δ'), (Zhu, et al., 2005). The melt contains mostly the δ' form, while isothermal crystallisation or slow cooling results in the α -form. When the α form is heated to above 95°C, an $\alpha \rightarrow \delta$ transition occurs. Such behaviour is characteristic to most polyamides and known as the Brill transitions.

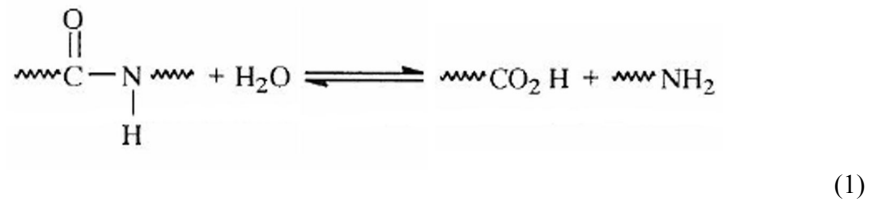
PA11 exhibits many different chain arrangements, which depend on the melt processing methods and parameters. Extrusion typically results in uniaxial orientation, whereas molding and casting yields planar orientation. Orientation of chain segments may also happen as a result of the uniaxial strain breaking up the spherullites and lamellae into individual chain segments, which subsequently arrange into newly oriented structures (Jolly, et al., 2002). The morphology of polymers plays a key role for their mechanical properties.

The mechanical behavior of polymers is complex and thus it is often explained by the combination of various thermodynamical, molecular and viscoelasticity theories; additionally fitted with the empirical parameters. Polyamides exhibit viscoelasticity characterized by the lack of linear behavior in the stress-strain curve. This behavior is a result of molecular relaxation in which the uncoiling of molecular chains reduces the stress required to obtain a certain strain. High strain rates give the chains less time for relaxation and stiffness of the material increases. Chain conformation, its length, branching, intra- and intermolecular bonding are all properties that affect the stress-strain correlation in the amorphous phase. Generally the tensile strength and elongation at break tend to increase with higher molecular weight and decrease with branching (Sperling, 2006).

Semicrystalline polymers can be modeled as two-phase composites with the crystalline phase corresponding to fibers the amorphous areas forming the matrix (Halpin & Kardos, 1972). Therefore the crystalline phase contributes to increased hardness and it improves chemical, thermal and creep resistance of the material. The amorphous phase is associated with impact resistance, flexibility and high elongation at break. It is a specific combination of these properties that makes PA11 being commonly used in the oil and gas industry.

2.3. Hydrolysis

Hydrolysis is the scission of chemical bonds by the addition of water. In the case of polyamide hydrolysis, the amide group is converted into a carboxylic acid and an amine (or ammonia). The general scheme for polyamide hydrolysis is shown below:



Hydrolysis is very often catalyzed by the presence of acid or base in the environment. Amide hydrolysis occurs when a nucleus-seeking agent (so called nucleophile e.g. water or hydroxyl ion) attacks the carbon of the carbonyl group. In acids, nucleophilic attack proceeds faster after the carbonyl group becomes protonated. In an aqueous base, the catalytic effect is present since hydroxyl ions are better nucleophiles than polar water molecules. Compounds with carboxylic acid groups are the products of both reactions.

With ongoing hydrolysis molecular weight of the polymer continuously decreases. However, after chain scission the acid end group can recombine with a nearby amine end group and start solid-state polymerization. Competition between water induced chain scission and repolymerization finally results in equilibrium at a certain molecular mass.

The kinetics of the reaction can be calculated after assuming a certain kinetic model, reaction rate constants and concentrations of reagents. The basic kinetic equation for hydrolysis of PA11 can be written as given in (**Jacques**, et al., 2002):

$$r(W) = \frac{dn}{dt} = k_H[\text{Amide}][\text{Water}] - k_R[\text{Acid}][\text{Amine}] \quad (2)$$

where: $r(W)$ is the rate of hydrolysis, k_H, k_R are the hydrolysis and recombination reaction constants.

More details regarding the chemistry of PA11 hydrolysis can be found in (**API**, 2003).

Hydrolysis is considered the most important ageing mechanism for polyamide elements working at elevated temperatures thus much effort has been put into experimental research. Moreover, several kinetic models predicting molecular weight evolution with time have been developed for the hydrolysis of polyamides: (**Jacques**, et al., 2002); (**Meyer**, et al., 2002) and (**EI-Mazry**, et al., 2012).

Hydrolysis has a dualistic effect on PA11 properties: chain scissions destroy the entanglement network in the amorphous phase (softening, brittleness, Tg decrease) and liberate small molecular segments which rearrange locally and initiate chemocrystallization (stiffening, Tg and density increase). However, in the case of polyamide 11 it has been also found that brittleness occurs suddenly at a critical molar mass M_F as a direct consequence of aging in water.

2.4. Empirical Service-Life Prediction

Today common practice is to evaluate degradation using accelerated aging at elevated temperature. Mechanical properties such as modulus, elongation at break or ultimate strength can be logged. Alternatively changes in molecular weight may be tracked, due to existence of the brittleness criterion $M_n < M_F$. Subsequently, the Arrhenius approach is used to analyze short-term high temperature aging data. Results are extrapolated and utilized to make long-term predictions for lower service temperatures.

The Arrhenius equation was originally developed in 1889 to describe the temperature dependence of the rate constant for an elementary chemical reaction:

$$k(T) = A \exp\left(-\frac{E_a}{RT}\right) \quad (3)$$

where: $k(T)$ is temperature dependent reaction rate, A is the temperature independent frequency factor, R is the universal gas constant and E_a is the Arrhenius activation energy, which is the minimal energy required to transform the reactants into products. The frequency factor expresses the total number of molecule collisions, while $\exp\left(-\frac{E_a}{RT}\right)$ is the probability that any given collision leads to a reaction.

In practice, even complex processes are often modeled as if they consisted of a single elementary reaction. This approach is widely used in chemical kinetics, as well as material and food science e.g. (**Petrou & Tampouris**, 2002) and (**Le Saux**, et al., 2014). In case the total reaction time of a certain process is known, such as the “embrittlement process”, the kinetic equation can be written as follows:

$$\ln t = \ln A' + \frac{E'_a}{R} \left(\frac{1}{T}\right) \quad (4)$$

After linear regression of the experimental data, $\frac{E'_a}{R}$ serves here as a slope of the $\ln t$ vs. $(\frac{1}{T})$ function and $\ln A'$ is its intercept. Thus they can be used to calculate the apparent activation energy E'_a and prefactor A' , respectively. Now all data needed for extrapolation to different temperatures is obtained. When the evolution curve of a certain property must be assessed shift factors are often defined instead, as shown in (**Le Saux**, et al., 2014):

$$a_T = \exp \left[\frac{E_a}{R} \left(\frac{1}{T_{ref}} - \frac{1}{T} \right) \right] \quad (5)$$

The reference temperature can be any temperature used in the test, typically it is the lowest one. Then the activation energy is found from a_T vs. $(\frac{1}{T})$ relationship and extrapolation to the service temperature can be completed.

The American Petroleum Institute (API) has developed the aging curves for PA11 degradation in different environments using the Arrhenius approach together with an empirical initial service acceptance criterion based on the Corrected Inherent Viscosity (CIV)= 1.2 dL/g. Figure 4 shows the time of degradation until the CIV value is reached.

The Arrhenius approach focuses exclusively on the macroscopic results. No consideration is given to microscopic mechanisms, which are behind the various degradation phenomena. Moreover, complex chemical processes are here grossly simplified. In reality, the chemical transformations at higher temperatures may be of a different nature than those occurring at lower temperatures (**Petrou & Tampouris**, 2002) leading to a temperature dependence of the activation energy E_a . Polymer science practice has also shown that the Arrhenius based evaluation cannot be used for bulk governed properties, such as elastic modulus and tensile strength, if a degradation gradient across the sample thickness exists, characterizing the diffusion limited degradation (**Le Saux**, et al., 2014).

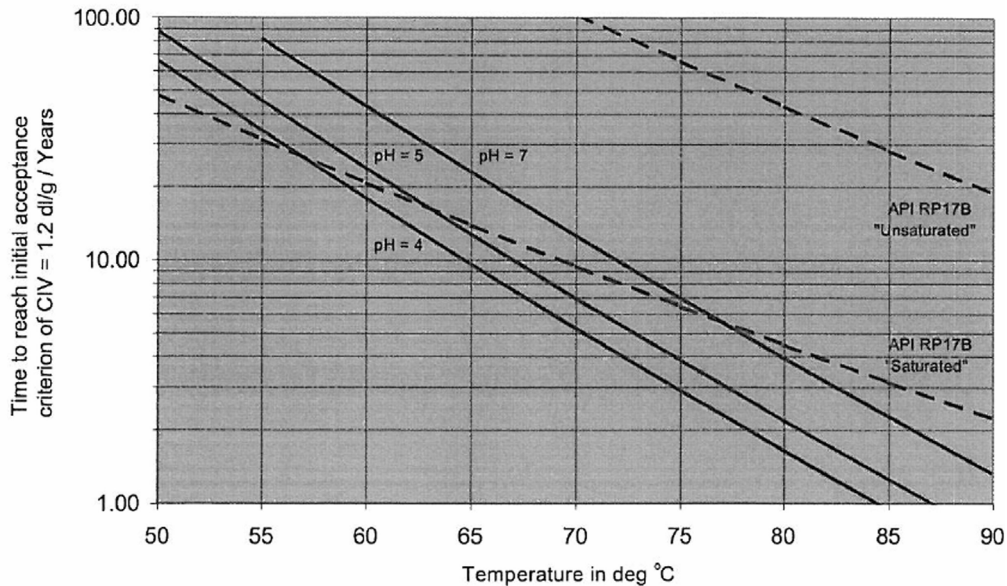


Figure 4. Arrhenius based aging curves for PA11 aging according to (API, 2003).

2.5. Multiscale modeling

Perceived flaws of the Arrhenius based evaluation led to development of alternative modeling approaches to predict the polymer degradation. Contrary to traditional models, multiscale modeling operates on multiple scales of resolution. Based on the review by (**Weinan & Jianfeng**, 2011) a summary of the key concepts of the multiscale approach is given in the following section.

A multiscale model integrates several single-scale models into one coherent framework. Individual models may originate from physical laws of different nature, for example, one from continuum mechanics and one from molecular dynamics. This is done to compromise between accuracy of microscale models and efficiency offered by the macroscale modeling.

Models operating in the macroscale make use of constitutive relations, which typically require analysis of the experimental data and making certain assumptions regarding the governing mechanism of the process. Making the right guess has proven to be remarkably effective as e.g. in the case of the Newton laws of mechanics. However, it has been also seen that formulating correct constitutive equations for complex systems (such as those in fluid dynamics) gets increasingly more difficult.

An alternative is to start right from the bottom and use the most fundamental properties of matter and force, as described by quantum mechanics. In order to obtain a complete model describing all of the phenomena in the natural science, at least from the reductionist perspective, it would be enough to input the atomic numbers of all the participating atoms and their potential energy model. However, for each additional particle used in the quantum mechanics based many-body problem the dimensionality of the problem increases by a factor

of three. In consequence, direct applications of the first principle are limited to very small spatial and temporal scales of resolution. Even in the case of a much more practical approach, such as the molecular dynamics, currently available computational power cannot provide simulations on the macroscopic scale (Buehler, 2008).

Multiscale modeling makes use of the best that both macro- and micro- scale models currently have to offer when it comes to engineering predictions. It consists of three interrelated activities:

- ❖ Multiscale analysis studies the relation between single-scale models, prospective to be included into the multiscale framework
- ❖ Scale-bridging focuses on procedures required to integrate these individual models
- ❖ Multiscale algorithms are required to practically implement the developed multiscale model

Figure 5 features the example of temporal and spatial hierarchy in the multiscale approach.

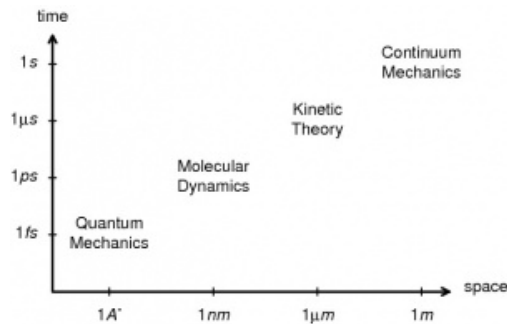


Figure 5. Practical hierarchy of models in the multi-physics approach. (Weinan & Jianfeng, 2011)

The multiscale models may be classified with regard to their internal structure and types of problems they are applied to. Sequential multiscale modeling gives a macroscale model in which some details of the constitutive relations are precomputed using microscale models. It is mostly limited to cases when only several quantities are passed between the macro and microscale models. In concurrent multiscale modeling, the parameters needed in larger scale model are obtained on-the-fly as the computation proceeds. For example, it is much more efficient to compute the inter-atomic forces on-the-fly from the first principle rather than precompute them. Multiscale modeling is mostly used for two types of situations. In the first one (type A), some interesting events, such as singularities, chemical reactions or crystalline defects, happen locally. Then a microscale model resolves the local behavior of these events, while bulk properties elsewhere are still described in terms of the macroscale model. In the second situation (type B) some constitutive information is required in the macroscale model and integrating with the microscale model supplies this missing information.

The bottom-up approach proposed in this thesis can be classified as type B, sequential multiscale model. It is divided into four fundamental stages:

- Evaluation of the environmental agents (water, oxygen, acids etc.) concentration profile in the polymer with time,
- Effect of chemical action of the environmental agent on the polymer molecular properties with time,
- Microstructure-property relationship yielding local mechanical properties of the polymer,
- Combining the local properties into global material properties.

3. Experimental Techniques & Materials

In this work the ageing process of PA11 was examined by tracking the changes of its mechanical properties. The mechanical test methods in question were tensile testing and dynamic mechanical thermal analysis (DMTA). The latter was performed to follow changes in the glass transition temperature and storage modulus. Weight measurements were performed to keep track on sample density and weight loss. Viscometric analysis determined the molecular weight after degradation. Thermal Gravimetric Analysis investigated plasticizer extraction and Differential Scanning Calorimetry crystallinity evolution. Experimental details are comprehensively described in Paper A. This chapter provides a short summary of that description.

3.1. Material

The polyamide 11 under study was Rilsan® BESNO TL40 from Arkema, which is widely used for offshore applications. The product specification states that this is an extrusion or blow molded PA11 with normal viscosity, no color additives, medium flexibility and added heat and light stabilizers (Arkema, 2012). The material contains nominally 12.5% N-butylbenzenesulfoneamide (BBSA) plasticizer. The plasticizer's molecular structure is shown in Figure 6.

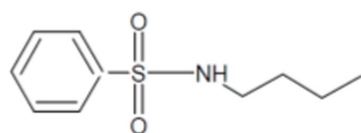


Figure 6. Molecular structure of BBSA plasticizer.

The samples were cut from an unused circular pressure sheath made for a flexible riser. Strips with a thickness of approximate 0.5 mm were cut from the pressure sheath in a manner so that the cross-section of the pressure sheath constituted the width of the strips.

3.2. Accelerated Aging

Ageing of the PA11 samples was performed in a 17 liter closed stainless steel 254 SMO autoclave. The thin sheet samples of 0.5 mm were thread onto a metal wire hanging from the lid of the autoclave ensuring exposure of the samples from both sides. The autoclave was filled with 15 liter distilled water. To prevent oxidative degradation processes the water was deoxygenized to a level of 2-4 ppb oxygen by bubbling with nitrogen gas (N_2 5.0) for approximately 20 hours. The autoclave was then placed on a plate heater and heated up to 120 °C as measured with a thermocouple inside the fluid chamber. The autoclave was opened for sample retrieval every week the first month, then every second week up to ten weeks. The oxygen content of the water at the end of each exposure period was measured with a Hach Orbisphere 410 sensor, which revealed no major changes. Every time the autoclave was opened the water was replaced and the nitrogen-bubbling routine repeated before the heat was turned on again.

3.3. Gravimetric Measurements

The density was found by Archimedes' principle. The mass of the samples in air and apparent mass upon immersion in water at 23°C was determined using an analytical balance with a sample holder. The specific gravity and density was calculated as described in the ASTM D792-08 Standard Test Methods for Density and Specific Gravity (Relative Density) of Plastics by Displacement (ASTM, 2008).

3.4. Volatile Extraction

For samples aged in oxygen-containing water at 90°C the amount of volatile compounds was determined by thermogravimetric analysis (TGA) in a nitrogen atmosphere using a Pyris 1 TGA from PerkinElmer. Samples were heated at 5°C/min from 20°C to 310°C. The mass loss between 30°C and 110°C was attributed to water loss and the mass loss between 110°C and 310°C was attributed to loss of plasticiser. The latter one can be therefore thought of as the remaining content of plasticizer in the sample after specified exposure time. The volatile content for samples aged in oxygen-free water in 90°C and 120°C was determined by mass loss after 90 minutes in a vacuum oven at 200°C.

3.5. Viscometric Analysis

The Inherent Viscosity IV was determined based on the description from (API, 2003). The PA11 was dissolved in *m*-cresol (C85727 99% solution from Sigma-Aldrich) to a concentration of 5.00 mg/cm³. The frequency dependent viscosity of the solution was measured using a plate-plate rheometer (Anton Paar MCR 300) in the frequency range 100 – 400 s⁻¹ and the average viscosity in this range is used to calculate the IV. The API 17TR2 specifies the use of a capillary rheometer for measuring the viscosity, but a plate-plate rheometer was used here to provide better control of the shear rate and temperature. Since PA11 used in flexible risers contains additives the measured IV needs to be corrected in order to obtain viscosity of pure PA11. According to (API, 2003), the Corrected Inherent Viscosity CIV is given by:

$$CIV = \frac{IV}{(1 - \text{extractable content})} \quad (6)$$

The relation between measured corrected inherent viscosity and weight-average molecular weight was calculated with the empirical relationship from (Jacques, et al., 2002):

$$CIV = 10^{(0.58121 \times \log(M_w) - 2.5595)} \quad (7)$$

where M_w is the weight-average molecular weight . The number average molecular weight M_n can be calculated with the formula:

$$M_n = \frac{M_w}{P_{di}} \quad (8)$$

where P_{di} is polydispersity index.

3.6. Differential Scanning Calorimetry (DSC)

DSC analyses were performed on a Perkin–Elmer Pyris Dynamic DSC with nitrogen as purge gas. Approximately 6 mg was weighed (+/- 0.001 mg) and placed in Al-pans. The samples were analysed with the following program:

1. Hold 30°C for 5 min
2. Heat 10°C/min to 225°C
3. Hold temperature for 5 min
4. Cool 10°C/min to 30°C
5. Hold temperature for 5 min
6. Heat 10°C/min to 225°C

Crystallinity changes in aged samples were determined with DSC analysis using the following formula from (**Sichina**, 2000):

$$\chi = \frac{dH_{melt, \text{ polymer}}/dH_{melt, \text{ crystal}}}{m_{vacuum, 200^\circ C}} \quad (9)$$

where χ is a degree of crystallinity, $dH_{melt, \text{ polymer}}$ is the melting enthalpy of the studied polymer, $dH_{melt, \text{ crystal}}$ is the melting enthalpy for pure crystalline phase, and $m_{vacuum, 200^\circ C}$ is the 1- extractables (water and plasticizer) ratio as measured after 90 minutes at 200 °C in a vacuum oven.

In addition to the standard method reported in literature e.g. by (**EI-Mazry**, et al., 2012) additive (plasticizer) extraction was also included in equation 9 to ensure that the heat of melting is related to the actual mass of the polymer.

3.7. Tensile Test

Measurements of stress vs. strain curves were made with a Schenck 10kN tensile-testing machine. The samples were 0.5 mm thick dumbbells shaped according to ISO 527 1BA. The tests started with a pre-strain from a load of 3N to avoid bias from strain in clamps or other parts of the instrument upon loading. The samples were stretched with a displacement rate of 2 mm/min until fracture or reaching 50% strain.

Stress-strain curves were obtained from the load displacement measurements. Two parameters from the stress-strain curves were evaluated: the Young's modulus and the tensile strength. The Young's modulus was derived from the slope between 0.2% and 0.5% strain of the stress-strain curves according to common practice in polymer science. In addition, the tangential modulus was measured as the local slope of the stress- strain curve for different strain levels. The tensile strength was calculated by dividing the maximum load in each stress-strain curve by the original cross sectional areas.

3.8. Dynamic Mechanical Thermal Analysis (DMTA)

The dynamic mechanical properties in flexure at the various stages in the ageing process were measured by dynamic thermal mechanical analysis (DMTA) in a Rheometrics Solids Analyzer RSA II. Sample bars with dimensions 0.5x6x50 mm were tested in a dual cantilever beam arrangement. The tests were run with 0.2% strain at a frequency of 1 Hz and a temperature sweep from 25 °C to 125 °C. The temperature steps were 4 °C and the soak time for each step was 120 seconds. The storage and loss modulus as well as $\tan \delta$ were logged. Three samples were analyzed for each withdrawal. It was revealed that the thin sheet samples lost a considerable amount of moisture during the relative short time it took to perform the mechanical tests. Therefore after aging in water at 120°C some samples were left drying for 48h in desiccator to ensure consistent conditions of the samples during testing.

4. Multiscale Model of PA11 Degradation

The multiscale approach is presented here as a way to improve the long-term property evaluations. Many models operating on individual stages of the proposed method exist already. Nevertheless so far the problem hasn't been treated holistically to form a multiscale model of degradation from the single-scale models. The purpose of this study is to change the state of the art in this research area by linking microscopic degradation induced by chemical factors to macroscale properties of the polymer.

4.1. General Description

Details of the model both in the general case and as applied to PA11 are presented in Paper B. The following section provides a short summary of this description. The input and output parameters of all constituent models used here for PA11 are presented in Paper B for morphological parameters and in Paper C in the case of the mechanical properties. Figure 7 presents a general scheme of the multiscale approach to degradation.

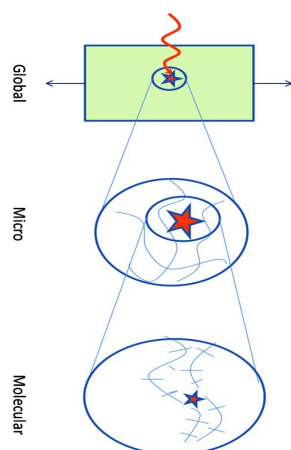


Figure 7. Multiscale approach combining macro-, micro- and molecular scales to evaluate degradation.

The multiscale model proposed here consists of four fundamental stages as described below:

➤ Stage 1: Concentration Profile

The concentration profile of the environmental agents (water, oxygen, acids etc.) in the polymer must be evaluated with time. Normally Fick's diffusion characteristic is assumed, however if the shape of the concentration profiles is of key importance the validity of this assumption should be checked.

Diffusion in polyamides is usually considered to follow Fick's law. The diffusion coefficient of water in Polyamide 11 was taken from (**Wu & Siesler**, 2003). Its value shows, that for PA11 aged in water diffusion proceeds very fast. Therefore the environmental agent is uniformly distributed within the material. Polyamide 11 will be here considered completely saturated and Stage 1 will not be considered any further.

➤ Stage 2: Kinetic Model – Molecular Level

The effect of chemical action of the environmental agent on the polymer molecular properties with time must be found. This is a key part of the methodology as it predicts the molecular response in the long-term perspective for which direct empirical evaluation would be impractical or impossible. The most important property changes addressed in this task are molecular weight decrease and degree of crystallinity increase, as described in Paper A.

The kinetic model by (**Jacques**, et al., 2002) was chosen to calculate the kinetics of hydrolytic chain-scission due to its confirmed accuracy and relative simplicity. Chain scissions result in decreased molecular weight, which in turn decreases stiffness in the amorphous phase and will eventually cause the embrittlement of the entire material (**Bicerano**, 2002).

The molecular weight evolution in Jacques kinetic model is governed by the following equation:

$$M_n(t) = M_{ne} \frac{M_{no}^{-1} + M_{ne}^{-1} + (M_{ne}^{-1} - M_{no}^{-1}) \exp(-Kt)}{M_{no}^{-1} + M_{ne}^{-1} - (M_{ne}^{-1} - M_{no}^{-1}) \exp(-Kt)} \quad (10)$$

where:

M_{ne} - equilibrium molecular mass,

M_{no} - initial molecular mass,

K – experimental pseudo rate constant.

The Jacques kinetic model is presented in more detail in Paper B as well as in the original reference.

Moreover the chain scissions tend to destroy the entanglement network in the amorphous phase and liberate small molecular segments, which diffuse towards the crystal's surface and initiate chemicrystallization (**El-Mazry**, et al., 2012). The Fayolle model, given in the former reference, predicts the degree of crystallinity as a function of aging time. Required input includes the initial crystallinity χ_{c0} , molecular weight evolution $M_n(t)$ and entanglement molecular weight M_e :

$$\chi(t) = \chi_{c0} + \frac{\frac{1-\chi_{c0}}{\frac{1}{2}}}{[\left(\frac{M_{no}}{M_n(t)}\right)^{\frac{1}{2}} - 1]} \left[\left(\frac{M_{no}}{M_n(t)}\right)^{\frac{1}{2}} - 1 \right] \quad (11)$$

➤ *Scale Bridging: Stage 2 to Stage 3*

Individual models are designed to function in a specific scale range. In order to couple single-scale models and develop larger multiscale model a *scale bridging* procedure is required. In the case of the degradation model proposed here only one such procedure is needed. The dependence of the glass transition temperature on molecular weight $T_g(M_n)$ must be found to integrate the kinetic model with the structure-property relationship. $T_g(M_n)$ can be obtained with the empirical equation described in (**Fox & Flory**, 1950) and (**Bicerano**, 2002):

$$T_g(M_n) \approx T_g^\infty - 0.002715 \frac{(T_g^\infty)^3}{M_n} \quad (12)$$

where: T_g^∞ is the hypothetical T_g for infinite molecular mass. T_g^∞ is a material parameter that can be calculated substituting initial T_g and M_n to the former equation.

➤ *Stage 3: Structure-Property Relationship*

A microstructure-property relationship yielding local mechanical properties of the polymer must be found. The topological method for the prediction of polymer properties is described in detail by (**Bicerano**, 2002). In the following paragraphs a very short summary of this description is given.

The multiscale approach proposed here used topological formalism utilizing connectivity indices defined via graph theoretical concepts as primary descriptors of the polymer repeat units. Topology can be seen as a pattern of interconnections between atoms in a polymer repeat unit. Connectivity indices give information on electronic configuration and coordination number for all atoms in the monomer.

In order to quantitatively predict polymer properties from the microstructural data connectivity parameters are correlated with the experimental results of so called *fundamental properties*. Fundamental material properties are properties in the microscale such as volume occupied by the molecule, cohesive energy etc. They are further combined into *derived properties* in the macroscale such as density or elastic constants. Formulas for derived properties are obtained by fitting the experimental data with equations from thermodynamic and molecular theories.

It is argued that this method is more practically feasible than alternative approaches e.g. molecular dynamics simulations or group contribution technique. Molecular dynamics must deal with time limitation and scale bridging issues (**Kremer & Müller-Plathe**, 2002). Group contribution technique cannot be used if estimating value of even a single group contribution is problematic. This serious limitation actually triggered development of the topological approach.

The structure of the PA11 repeat unit was analyzed to obtain the topology data. The following values of the connectivity indices were found and will be used in the model:

$$\begin{aligned} X_0 &= 9.3555, & X_0^V &= 8.4793 \\ X_1 &= 6.3938, & X_1^V &= 5.6612 \end{aligned} \quad (13)-(16)$$

Generally X_0 and X_1 provide information on coordination numbers, while X_0^V and X_1^V quantify details of the electronic configuration in the monomer.

The exact procedures required to get the structure-property relationships in the Stage 3 are different for each property to be obtained. They are described in detail for the mechanical properties in Paper C. The model for morphology predictions is featured in Paper B.

➤ Stage 4: Global Properties

In the final stage the local properties must be combined into global engineering parameters. This can be done with several methods such as micromechanical Finite Element Analysis or composites theory, e.g. (**Halpin & Kardos**, 1972).

In the case of PA11 aging described here there is an even distribution of water through the body as the diffusion happens very quickly. Besides this the current modeling approach has seen the amorphous matrix as perfectly homogenous with evenly distributed crystallites. Therefore properties will be uniform throughout the material and global engineering properties do not need to be evaluated. Because of this Stage 4 will not be considered at any point later in the dissertation.

4.2. Discussion

The model proposed here for the prediction of morphological parameters is not only accurate, but also particularly simple to use due to the analytic form of its expressions. Therefore it can be easily programmed in languages such as MATLAB, calculated in Excel spreadsheets or even typed into a handheld calculator (**Bicerano**, 2002). The predictive power of the model was demonstrated here in the case of PA11 hydrolytic degradation. The model can be applied to any other polymer providing that input parameters for diffusion and structure property models are known and a kinetic model for the specific chemical process in the specific material can be found. The latter somewhat limits the generality of the proposed approach. However, in practice, the kinetic models providing $M_n(t)$ as an output have been developed whenever it was required by industry (**Fayolle**, et al., 2008). Consequently such models exist for a wide range of practically important chain-scission processes in different materials.

Input parameters for the property predictions can be obtained relatively easy. Data required for structure-property relationship of the amorphous phase (connectivity, mass and length of the polymer repeat unit) can be directly calculated from the structure of the monomer. The density of the crystalline phase φ_c and the glass transition temperature T_g are also material constants and can be found in the literature for many polymers. Sample-dependent parameters such as initial molecular weight M_{n0} and initial degree of crystallinity χ_{c0} may also, in the

first approach, be taken from the literature for a “typical sample” or ideally be obtained experimentally for the studied specimen. This can be done with viscometric and spectrometric measurements for M_{n0} or by XRD, DSC, FTIR and density tests for χ_{c0} . Among the mentioned parameters initial crystallinity appears to be the most difficult to find in the literature. It may be available with good accuracy only for common polymers and is highly dependent on process history. The quantities such as modulus of the crystalline phase E_c and characteristic ratio of macromolecules C_∞ are more difficult to find for every polymer. In this case, as a practical approach, values for closest known material should be assumed. Here the crystalline modulus of commonly used PA6 was taken as a proxy for PA11.

The proposed multiscale model allows obtaining property predictions based on the actual structure of the polymer and is therefore a step forward compared to simple and completely empirical extrapolation of the experimental tests results used today. This model is based on molecular processes although it is still a semi-empirical approach, which relies heavily on correlations to obtain properties in the amorphous phase. Consequently the model cannot provide any theoretical understanding of property emergence from the structure in the microscale. It did however bring some insights into behavior on larger scales, e.g. it evaluated the role of crystallites in the plastic deformation and proposed the existence of a mechanical equilibrium. The theory does not account for the modulus strain rate dependence, which corresponds to testing at the arbitrary "standard" rate. Predictions may therefore deviate from experiment in extreme cases, however high accuracy has been obtained in the literature for commonly used loading rates (**Bicerano**, 2002). Moreover, the model ignores any possible effects of parameters like crystallite size, distribution and orientation or molecular weight distribution. It should be possible to develop the model further and consider these effects in detail. Predictions should also improve once better input data is available. Nevertheless, the good match between model and experiment indicates that the approach taken here is sufficiently accurate for Polyamide 11. It is therefore a framework to build on for future generations of the multiscale models.

The model does not have any theoretical basis to evaluate the effects of plasticizers and it is best applicable to dried specimens. Nevertheless for important polymers, water absorption (acting as plasticizer) and plasticizer extraction have been linked to changes of the mechanical properties, as described in (**Silva**, et al., 2013) and (**Arkema**, 2012), respectively. Therefore, empirical softening factors can be used to estimate the properties of water saturated samples with residual plasticizer content in place. Results for Polyamide 11 suggest that this produces predictions relevant from a practical point of view.

Generally the model should be understood as a practical tool aiding engineers with fast and accurate predictions of the morphology and resulting mechanical properties.

5. Summary of Papers

In this section a summary of the published papers is given. Abstract and conclusions for each article are provided.

Paper A. Aging of Polyamide 11. Part 1: Evaluating degradation by Thermal, Mechanical and Viscometric Analysis.

Hydrolytic degradation at elevated temperatures is a key reason for failure in offshore flexible risers. In this paper the ageing of polyamide 11 in deoxygenated water at 90 °C and 120 °C was studied. Tensile and DMTA tests were performed to measure changes in mechanical properties. Viscometry, gravimetric measurements, DSC and TGA were used to link these properties with morphological changes.

General trends are increased stiffness, tensile strength and glass transition temperature as well as decreased glassy state damping efficiency with increased ageing times. Changes can be initially ascribed to plasticizer depletion and then to interplay between molecular weight decrease and crystallinity increase. Viscosity at hydrolysis equilibrium indicates that brittle failure typically involves oxidation or UV exposure.

Conclusions of Paper A:

Paper A revealed that there are four main mechanisms of property change. Plasticizer extraction contributes to stiffening of the material (modulus and strength increase), T_g increase and density decrease- partially diminished by water absorption acting as plasticizer. Moreover hydrolysis has a dualistic effect on properties: chain scissions destroy the entanglement network in the amorphous phase (softening, embrittlement, T_g decrease) and liberate small molecular segments, which rearrange locally and initiate chemicrystallisation (stiffening, T_g and density increase). Experimental results regarding changes in morphology and properties of PA11 under hydrolytic degradation in 120°C have been compared and the main findings are listed as follows:

- ❖ Occurrence of brittle failure by hydrolysis only is rare and typically involves additional mechanisms of chain scission e.g. oxidation or UV exposure
- ❖ Mechanical properties evolution can be divided into three control domains for thin PA11 materials:
 1. *Plasticizer control* during the first 2 weeks, stiffness and strength show a rapid increase
 2. *Chemicrystallisation control* in the following month, stiffness and strength show a moderate increase
 3. *Plateau region* after about 6 weeks, stiffness and strength exhibit an infinitesimal increase
- ❖ The glass transition temperature increases as the degradation proceeds, contrary to the Fox and Flory theory for amorphous regions. It can be explained by the fact, that amorphous chain segments get constrained by the immobile crystallites following chemicrystallisation

Further conclusions from the experimental study can be listed as follows:

- ❖ PA11 sinks in water at all aging times. The ultimate density is close to the initial one
- ❖ Damping efficiency (loss of tangent modulus measured by DMTA) is affected negatively by degradation for samples in the glassy state, but not in rubbery state
- ❖ The presence of water contributes to the decrease of both glass transition temperature and damping efficiency

Paper B. *Aging of Polyamide 11. Part 2: General multiscale model of the hydrolytic degradation applied to predict the morphology evolution.*

Accelerated aging tests are the conventional way to evaluate long-term degradation of polymers, in particular for offshore flexible risers. In this paper a multiscale model has been developed combining diffusion, chemical kinetic reactions, structure-property relationships and composite models to provide faster and less labor extensive property predictions. A general methodology is presented and applied to predict the density and crystallinity evolution. Results are compared with experimental ageing of polyamide 11 in deoxygenated water at 120 °C.

For both density and degree of crystallinity the modeled trend is close to the experimental test results. Accurate prediction of the morphological parameters during degradation allows extension of the multiscale model for the prediction of mechanical properties.

Conclusions of Paper B:

In Paper B a general multiscale methodology for property predictions under aging is presented. Multiscale modeling results for the morphological properties of PA11 are compared with aging tests performed in water at 120°C. A very good match between model and experiment is obtained for both the density and degree of crystallinity. The model is easy to use, using simple semi-empirical formulas, once the fundamental input parameters are obtained. The fundamental parameters can be found for most common polymers in the literature. The effect of depletion of plasticizer and low molecular weight components is not modeled and needs to be evaluated separately. This effect is however irrelevant for crystallinity predictions and in the case of PA11 density may only be important in the first two weeks of exposure. The successful prediction of PA11's structural parameters during degradation opens the possibility to predict engineering mechanical properties.

Paper C. *Aging of Polyamide 11. Part 3: Multiscale model predicting the mechanical properties after hydrolytic degradation.*

A holistic general multiscale model of polymer degradation has been applied to predict the mechanical properties of polyamide 11 after the hydrolytic ageing. Results for elastic modulus, tensile strength and brittleness threshold have been compared with experimental aging in deoxygenated water at 120°C.

For all studied properties the modeled trend is close to the experimental test results confirming hydrolysis induced chain scission and chemicrystallisation as the two main mechanisms of property change. This suggests that the multiscale modeling methodology can provide a valuable alternative to accelerated aging tests. Moreover, the model indicated that

the crystalline phase does play a role in plastic deformation and it detected the existence of the mechanical equilibrium between effects of macromolecule degradation and an increased degree of crystallinity.

Conclusions of Paper C:

In Paper C the mechanical properties were predicted from previously modeled morphological parameters. For all three; the tensile yield strength, storage modulus and embrittlement threshold; prediction of the model is close to the experimental results. This similarity confirms that the modeling approach chosen here gives relevant results. It also confirms that hydrolysis induced chain scission and chemocrystallisation are the two main mechanisms of property change, because these two mechanisms are central to all modeling used. Results for the tensile strength suggest that the crystalline phase does play a role in plastic deformation as opposed to the view that this is solely a matter of the amorphous phase. The model detected the existence of mechanical equilibrium between effects of macromolecule degradation and increased degree of crystallinity. The multiscale model developed in this work is easy to use, using simple semi-empirical formulas, once the fundamental input parameters are obtained. The fundamental parameters can be found for most common polymers in the literature. The model provides a faster and less labor extensive engineering alternative to accelerated aging tests.

6. Concluding Remarks

This thesis focused on developing the multiscale model of the Polyamide 11 hydrolytic degradation in order to improve cost, accuracy and generality of property predictions comparing to accelerated aging tests.

The experimental part of this work investigated the link between mechanical behavior and morphology of PA11 during degradation through use of tensile testing, Dynamic Mechanical Thermal Analysis and material characterization techniques. Several interesting conclusions have been drawn from this study. The most important is identification of the main mechanisms of property change. These are plasticizer extraction, water saturation and hydrolysis. Hydrolysis has a dualistic effect on properties: chain scissions destroy the entanglement network in the amorphous phase (softening, embrittlement, T_g decrease) and liberate small molecular segments, which rearrange locally and initiate chemicrystallisation (stiffening, T_g and density increase).

Experimental results obtained here were compared with a multiscale model for PA11 hydrolytic degradation in the case of morphology evolution and mechanical properties. A good match between model and experiment clearly indicate that the multiscale modeling methodology can provide faster and less labor extensive alternatives to the common Arrhenius based extrapolation, when it comes to long-term property evaluation.

6.1. Future work

The multiscale model presented in this thesis is a practical tool aiding engineers with fast and accurate predictions of the morphology and resulting mechanical properties. In this work the most fundamental parameters were identified. The monomer architecture distinguishes one polymeric compound from the other. Average molecular weight is widely used to evaluate degradation (if only one parameter can be obtained, it is MW). The composite models of polymeric materials may ignore some parameters, but they always include the degree of crystallinity. In addition, the shape of crystallites was described here by a simplified geometry and taken into account. The results show that the simple approach taken here is sufficiently accurate for PA11. It can be therefore used as a framework to build on for future generations of the multiscale models.

In order to develop the model further and improve its predictive power following steps could be potentially taken:

- ❖ Providing more accurate input data
- ❖ Addressing effects of crystallite size, distribution and orientation
- ❖ Consideration of the full distribution of the macromolecule mass
- ❖ Including viscoelastic effects (chiefly strain-rate dependence)
- ❖ Developing theoretical basis for the effects of plasticizer depletion and water saturation
- ❖ Gradually moving from a semi-empirical to a fully theoretical approach

The model developed here suggests that the crystalline phase does play an important role in the plastic deformation as opposed to the view that this is solely a matter of the amorphous phase. The above hypothesis could be experimentally tested in the future by quantitatively comparing the shape of crystallites in undeformed and deformed samples.

As for the experimental study, observing changes of the microstructure in detail, e.g. with a scanning electron microscopy (SEM) and further image analysis, would provide parameters like crystallite size, shape, distribution and orientation to supplement the information given by degree of crystallinity. Moreover, size-exclusion chromatography (SEC) could be used to study molar mass distribution of the polymer. Such studies should be performed in the future to improve the understanding of the underlying phenomena and the model predictions.

7. References

- 4Subsea AS, 2013. *PSA no. 0389-26583-U-0032, Revision 5: Un-bonded Flexible Risers - Recent Field Experience and Actions for Increased Robustness*, Norway: 4Subsea AS.
- API, 2003. *API TECHNICAL REPORT 17TR2: The Ageing of PA-11 in Flexible Pipes*, Washington, D.C: API Publishing Services.
- API, 2008. *API RECOMMENDED PRACTICE 17B: Recommended Practice for Flexible Pipe*, Washington, D.C: API Publishing Services.
- Arkema, 2012. *Rilsan® PA11: Created From a Renewable Source*, France: Arkema.
- ASTM, 2008. *ASTM D792-08, Standard Test Methods for Density and Specific Gravity (Relative Density) of Plastics by Displacement*, United States: ASTM.
- Berggren R., 2013. *Long term degradation of polymers - Molecular and macroscopic effects*. Trondheim: Norwegian University of Science and Technology.
- Bicerano J., 2002. *Prediction of polymer properties*. New York: Marcel Dekker AG.
- Buehler M. J., 2008. *Atomistic Modeling of Materials Failure*. New York: Springer LLC.
- El-Mazry C., Correc O. & Colin X., 2012. *Polymer Degradation and Stability*, Volume 97, p. 1049.
- Fayolle B., Richaud E., Colin X. & Verdu J., 2008. *Journal of Materials Science*, Volume 43, p. 6999.
- FlexiRiserTest, 2010. *FlexiRiserTest*. [Online] Available at: http://www.flexirisertest.com/home/fig_2_1.html [Accessed 19 08 2015].
- Flynn J. H., 1995. *Journal of Thermal Analysis and Calorimetry*, Volume 44, p. 499.
- Fox, T. & Flory, P. J., 1950. *Journal of Applied Physics*, Volume 21, p. 581.
- Halpin J. C. & Kardos J. L., 1972. *Journal of Applied Physics*, Volume 43, p. 2235.
- Jacques, B. et al., 2002. *Polymer*, Volume 43, p. 6439.
- Jolly L., Tidu A., Heizmann J. & Bolle B., 2002. *Polymer*, Volume 43, p. 6839.
- Kohan M., 1995. In: *The Crystalline State. Nylon plastics handbook*. Munich: Hanser Publishers, pp. 239-324.
- Kremer K. & Müller-Plathe F., 2002. *Molecular Simulation*, Volume 28, p. 729.
- Le Saux V., Le Gac P., Marco Y. & Calloch S., 2014. *Polymer Degradation and Stability*, Volume 99, p. 254.

LookChem, 2008. *LookChem*. [Online] Available at: <http://www.lookchem.com/cas-250/25035-04-5.html> [Accessed 16 09 2015]

Meyer A., N. J., Lin Y. & Kranbuehl D., 2002. *Macromolecules*, Volume 35, p. 2784.

Petrou A., R. M. & Tampouris, K., 2002. *Chemistry Education Research and Practice*, Volume 3, p. 87.

Sichina W., 2000. *DSC as Problem Solving Tool: Measurement of Percent Crystallinity of Thermoplastics*. PETech-40 Thermal Analysis, United States: PerkinElmer.

Silva L., Tognana S. & Salgueiro W., 2013. *Polymer Testing*, Volume 32, p. 158.

Simonsen A., 2014. *Inspection and monitoring techniques for un-bonded flexible risers and pipelines*. Stavanger: University of Stavanger.

Sperling L., 2006. In: *Mechanical behavior of polymers. Introduction to physical polymer science*. New Jersey: John Wiley & Sons, Inc., pp. 557-612.

Weinan E. & Jianfeng L., 2011. *Scholarpedia*, Volume 6, p. 11527.

Wu P. & Siesler H. W., 2003. *Chemistry of Materials*, Volume 15, p. 2752.

Zhu J., X.Y., Z. & He B., 2005. *Space charge detrapping behavior in different crystal phase of nylon 11*. Bahia, ISE-12: 12th International Symposium on Electrets.

PART II

INCLUDED PAPERS

PAPER A

Tobiasz Mazan, Randi Berggren, Jens Kjær Jørgensen and Andreas Echtermeyer

Aging of Polyamide 11. Part 1: Evaluating degradation by Thermal, Mechanical and Viscometric Analysis

Journal of Applied Polymer Science, Volume 132, Issue 20, pages 6249-6260; Feb 19, 2015

Aging of polyamide 11. Part 1: Evaluating degradation by thermal, mechanical, and viscometric analysis

Tobiasz Mazan,¹ Randi Berggren,¹ Jens Kjær Jørgensen,² Andreas Echtermeyer¹

¹Department of Engineering Design and Materials, Norwegian University of Science and Technology, Trondheim 7034, Norway

²SINTEF Materials and Chemistry, Oslo 0373, Norway

Correspondence to: T. Mazan (E-mail: tobiasz.mazan@ntnu.no)

ABSTRACT: Hydrolytic degradation at elevated temperatures is a key reason for failure in offshore flexible risers. In this article, the aging of polyamide 11 in deoxygenated water at 90°C and 120°C was studied. Tensile and dynamic mechanical thermal analysis tests were performed to measure changes in mechanical properties. Viscometry, gravimetric measurements, differential scanning calorimetry, and thermogravimetric analysis were used to link these properties with morphological changes. General trends are increased stiffness, tensile strength, and glass transition temperature as well as decreased glassy state damping efficiency with increased aging times. Changes can be initially ascribed to plasticizer depletion and then to interplay between molecular weight decrease and crystallinity increase. Viscosity at hydrolysis equilibrium indicates that brittle failure typically involves oxidation or UV exposure. © 2015 Wiley Periodicals, Inc. *J. Appl. Polym. Sci.* **2015**, *132*, 41971.

KEYWORDS: crystallization; degradation; mechanical properties; oil and gas; polyamides

Received 12 September 2014; accepted 6 January 2015

DOI: 10.1002/app.41971

INTRODUCTION

Polyamides PA are known to undergo chemical degradation if they are exposed to oil and gas field exploration environments. The degradation leads to loss of mechanical properties and subsequently affects the lifetime of the given structure.¹

A very important application for PA is flexible risers. Oilfield flexible risers convey high temperature production fluids (typically mixtures of oil, gas, and water) from subsea units on the seabed to topside platforms. The risers are multilayered pipes of metal and polymers designed to have high axial stiffness and rather low bending stiffness. They have an internal polymer sheath to keep the transported fluid inside the pipe. Unbonded metal strips are wound around this sheath (in so called annulus) to provide strength and stiffness. An outer thermoplastic sheath is a barrier against seawater ingress. More details and drawing can be found in API 17B.²

The offshore environment presents many structural challenges to the flexible risers, such as the fluctuating dynamic loads imposed by surface waves and underwater currents. The polymer sheaths do not provide any structural strength, but they need to follow all deformations of the structure over its entire

life. This means they need a fairly high strain to failure (a few %) and good fracture toughness. Strength and stiffness of the polymer sheath are needed to bridge the gaps between the metal parts and to prevent excessive creep into the gaps.

Polyamide 11 (PA11) is one of the most common materials used for the internal pressure sheaths in flexible risers due to good fatigue and creep resistance as well as decent barrier properties toward oil and natural gas.³ Among the production fluids crude oil and gas cause mainly swelling of the polymer, therefore the transported high temperature water is a primary reason for degradation of PA11 internal pressure sheath. The structural integrity of this element is of great importance for environmental, economical and safety reasons. Nevertheless, almost 20% of the flexible pipe failure incidents in United Kingdom and Norway are related to aged internal sheaths.⁴

Industry and academic research have given aging of polyamides much attention over the past decades. Numerous aging experiments have been conducted on polyamides in different environments. Most studies used the decreasing molecular weight of the polymer chains as an indicative property of aging that can be related to the fracture toughness or failure strain of the material.^{1,5} Much effort has also been put into creating

Additional Supporting Information may be found in the online version of this article.

© 2015 Wiley Periodicals, Inc.

degradation models based on hydrolysis, which is established as the governing chain scission mechanism for PA11 in water at elevated temperatures.^{6,7} Still, the aging process of polyamides is complex and looking at the molecular weight reduction alone does not give an adequate overview of the material degradation. In addition to chain scission due to chemical reactions there are structural changes from annealing upon heating and chemicrystallization, as well as swelling by water uptake and plasticizer loss. These two last processes cause structural changes that are not detectable by molecular weight measurements, but may drastically affect the mechanical properties of the polyamide. Some investigations go a step further reporting additional morphological parameters and final properties such as degree of crystallinity,^{8,9} glass transition temperature,¹⁰ modulus,^{10,11} or plasticizer content.^{9–11} None of them however treat all these effects simultaneously and they don't consider additional quantities reported in this work such as density, water uptake, tangential modulus, tensile strength, and damping efficiency. The correlation between aging and changes in mechanical properties for PA11 is thus neither extensively described nor understood.

The purpose of this work was to investigate in detail the mechanical and volumetric properties of PA11 during degradation as well as the correlation between them and key morphological parameters. Accelerated aging tests were performed in oxygen depleted water at 90°C and 120°C. Contrary to many of the previous publications^{9–11} full evolution of each property up to 10 weeks of aging was reported, which is of particular importance for comparing experiments with degradation model predictions—the second part of our “Aging of Polyamide 11” study.¹²

EXPERIMENTAL

In this work the aging process of PA11 was examined by tracking the changes in mechanical properties. The mechanical test methods in question were tensile testing and dynamic mechanical thermal analysis (DMTA). The latter was performed to follow changes in the glass transition temperature and storage modulus. Weight measurements were performed to keep track on sample density and weight loss. Thermal gravimetric analysis investigated plasticizer extraction and differential scanning calorimetry (DSC) crystallinity evolution.

Material

The PA11 under study was Rilsan® BESNO TL40 from Arkema, which is widely used for offshore applications. The Arkema product specification states that this is an extrusion or blow molded PA11 with normal viscosity, no color additives, medium flexibility and added heat and light stabilizers.³ The material contains nominally 12.5% N-butyl-benzenesulfonamide (BBSA) plasticizer.

Specimen Preparation. The samples were cut from an unused circular pressure sheath made for a flexible riser. Strips with a thickness of approximate 0.5 mm were cut from the pressure sheath in a manner so that the cross-section of the pressure sheath constituted the width of the strips. Thin specimens were used to bring out the effects of plasticizer loss and water penetration quickly. Moreover both aging and plasticizer content

becomes more homogenous for thin sheet samples. Specimens for tensile testing and dynamic mechanical analysis were punched or cut from the strips after exposure since the thin samples tend to deform during aging. This procedure ensured an uniform sample geometry for the mechanical tests. For material aged 3 weeks or more surface cracks were observed on the dumbbells for tensile testing. These cracks were initiated when the samples were punched out from the strips. The cracks could potentially reduce the strength of a brittle material, however we have assumed their effect is negligible in the case of ductile material. This study also focused more on the shape of the stress vs. strain curve than the absolute strength, making crack development not so critical.

Accelerated Aging

Internal pressure sheath PA11 in operative risers is exposed to an oxygen free environment.⁷ In order to perform experiments as close as possible to these conditions oxygen had to be removed from the accelerated aging environment. Testing in oxygen free water is also interesting from a theoretical point of view, because it allows studying aging due to H₂O without any influence from oxygen.

Samples analyzed with DSC were aged with initially developed procedure. In the initial procedure a thin sheet samples of 100 mg were cut out and placed in a 20-mL vial (Part no. 354833 from Biotage). Then 20 mL deionized water was added. The liquid to sample volume ratio was between 25 and 200. The liquid had been deoxygenated by bubbling through Argon 6.0 for 3 h and the vial was flushed with Argon before adding the liquid. The vials were sealed and placed in a heating oven at a designated temperature for a preset time, up to 32 days. The vials were only opened after completed aging. No discoloration of samples was observed indicating that deoxygenation was satisfactory. Nevertheless it was decided to improve the aging procedure for mechanical, gravimetric, and viscometric tests. The new procedure allowed for a better oxygen and temperature control in the process, but otherwise it introduced no major differences.

Aging of the PA11 samples with improved procedure was performed in a 17-L closed stainless steel 254 SMO autoclave. The thin sheet samples of 0.5 mm were thread onto a metal wire hanging from the lid of the autoclave ensuring exposure of the samples from both sides. The autoclave was filled with 15 L distilled water. To prevent oxidative degradation processes the water was deoxygenated to a level of 2–4 ppb oxygen by bubbling with nitrogen gas (N₂ 5.0) for approximately 20 h. The autoclave was then placed on a plate heater and heated up to 120°C as measured with a thermocouple inside the fluid chamber. The autoclave was opened for sample retrieval every week the first month, then every second week up to 10 weeks. The oxygen content of the water at the end of each exposure period was measured with a Hach Orbisphere 410 sensor, which revealed no major changes. Every time the autoclave was opened the water was replaced and the nitrogen-bubbling routine repeated before the heat was turned on again.

Choice of Aging Parameters. The choice of times and temperatures for the aging tests in this study was based on the

hydrolytic degradation model proposed by Jacques.⁷ Industry practice requires that the corrected inherent viscosity (CIV) does not drop below 1.2 dL/g.¹ As given by the Jacques relationship in eq. (2) the acceptance criteria corresponds to M_w of 34.7 kg/mol and should be reached after about 5 weeks in water at 120°C.⁷ According to Jacques the molecular weight should drop further until it becomes stable after 7 weeks at 120°C. The aging was run up to 10 weeks to make sure the equilibrium was reached.

Material Storage and Handling

Density and DMTA measurements were performed on the aged (water saturated) samples the same day as they were withdrawn from the water bath. Due to difficulties with the equipment, samples for the other characterization methods were tested at a later time. To ensure that the aged material did not change before characterization the samples were put in distilled water in glass bottles and stored in a refrigerator. Some of the samples were placed in desiccator at room temperature 48 h prior to the tensile tests to remove moisture, others were tested in saturated state.

Material Analysis

Gravimetric Measurements. The density was found by Archimedes' principle. The mass of the samples in air and apparent mass upon immersion in water at 23°C was determined using an analytical balance with a sample holder.

The specific gravity and density was calculated as described in the ASTM D792-08 Standard Test Methods for Density and Specific Gravity (Relative Density) of Plastics by Displacement.¹³

Volatile Content. Fourier transform infrared spectroscopy (FTIR) measurements were performed for reference sample and one aged 20 days in 90°C. However, no significant change in spectra was observed and finally sample mass loss at elevated temperature was chosen as preferred method to determine amount of extractables. For samples aged in oxygen-containing water at 90°C the amount of volatile compounds was determined by thermogravimetric analysis (TGA) in a nitrogen atmosphere using a Pyris 1 TGA from PerkinElmer. Samples were heated at 5°C/min from 20°C to 310°C. The mass loss between 30°C and 110°C was attributed to water loss and the mass loss between 110°C and 310°C was attributed to loss of plasticiser. The latter one can be therefore thought of as the remaining content of plasticizer in the sample after specified exposure time. The volatile content for samples aged in oxygen-free water in 90°C and 120°C was determined by mass loss after 90 min in a vacuum oven at 200°C.

Corrected Inherent Viscosity. The inherent viscosity IV was determined based on the description from API 17TR2.¹ The PA11 was dissolved in *m*-cresol (C85727 99% solution from Sigma-Aldrich) to a concentration of 5.00 mg/cm³. The frequency dependent viscosity of the solution was measured using a plate-plate rheometer (Anton Paar MCR 300) in the frequency range 100–400 s⁻¹ and the average viscosity in this range is used to calculate the IV. The API 17TR2 specifies the use of a capillary rheometer for measuring the viscosity, but

a plate-plate rheometer was used here to provide better control of the shear rate and temperature. Since PA11 used in flexible risers contains additives the measured IV needs to be corrected in order to obtain viscosity of pure PA11. The CIV is given by¹:

$$\text{CIV} = \frac{\text{IV}}{(1-\text{extractable content})} \quad (1)$$

Present data consists of single measurements.

Relation Between CIV and Molecular Weight. The relation between measured CIV and weight-average molecular weight was calculated with Jacques empirical relationship similar to Mark-Houwink equation, however operating directly on M_w and not on viscosity-average molecular weight:

$$\text{CIV} = 10^{(0.58121 \times \log(M_w) - 2.5595)} \quad (2)$$

where M_w is the weight-average molecular weight.⁷ The number average molecular weight M_n can be calculated with the formula:

$$M_n = \frac{M_w}{P_{di}} \quad (3)$$

where P_{di} is polydispersity index.

PA11 is a polycondensate therefore its polydispersity index shall be close to 2.¹⁴ Previous studies reported no significant polydispersity change on degraded samples.⁷

Differential Scanning Calorimetry. DSC analyses were performed on a Perkin-Elmer Pyris Dynamic DSC with nitrogen as purge gas. Approximately 6 mg was weighed (± 0.001 mg) and placed in Al-pans. The samples were analyzed with the following program:

1. Hold 30°C for 5 min
2. Heat 10°C/min to 225°C
3. Hold temperature for 5 min
4. Cool 10°C/min to 30°C
5. Hold temperature for 5 min
6. Heat 10°C/min to 225°C

Degree of Crystallinity Measurement. Crystallinity changes in aged samples were determined with DSC analysis using the following formula¹⁵:

$$\chi = \frac{dH_{\text{melt, polymer}}/dH_{\text{melt, crystal}}}{m_{\text{vacuum}, 200^\circ\text{C}}} \quad (4)$$

where χ is a degree of crystallinity, $dH_{\text{melt, polymer}}$ is the melting enthalpy of the studied polymer, $dH_{\text{melt, crystal}}$ is the melting enthalpy for pure crystalline phase, and $m_{\text{vacuum}, 200^\circ\text{C}}$ is the 1—extractables (water and plasticizer) ratio as measured after 90 min at 200°C in a vacuum oven.

In addition to the standard method reported in literature^{8,15,16} additive (plasticizer) extraction was also included in eq. (4) to ensure that the heat of melting is related to the actual mass of the polymer. The present study followed approximation used in El-Mazry's work.⁸ It was assumed that the secondary lamellae possess the physical and thermal characteristics of the initial primary lamellae. Enthalpy was taken as an average of values obtained after first and second heating run.

Tensile Test

Measurements of stress vs. strain curves were made with a Schenck 10kN tensile-testing machine. The samples were 0.5 mm thick dumbbells shaped according to ISO 527 1BA. The tests started with a prestrain from a load of 3 N to avoid bias from strain in clamps or other parts of the instrument upon loading. The samples were stretched with a displacement rate of 2 mm/min until fracture or reaching 50% strain.

Choice of Tensile Properties. Stress-strain curves were obtained from the load displacement measurements. Stresses were calculated based on the initial cross-section of the samples in the thin part of the dumbbell specimens. Strains were calculated from the original length of the samples and machine displacement. This approach is not ideal, but the relative change between samples of different aging can be obtained fairly well. Two parameters from the stress-strain curves were evaluated: The Young's modulus and the tensile strength. The Young's modulus was derived from the slope between 0.2% and 0.5% strain of the stress-strain curves according to common practice in polymer science. This relatively broad measurement range should account well for the nonlinearity of the material. In addition, the tangential modulus was measured as the local slope of the stress-strain curve for different strain levels. The tensile strength was calculated by dividing the maximum load in each stress-strain curve by the original cross-sectional areas. True stress would be better for necked samples, but equipment to measure it in such small specimens was not available.

Dynamic Mechanical Thermal Analysis

Saturated Samples. The dynamic mechanical properties in flexure at the various stages in the aging process were measured by DMTA in a Rheometrics Solids Analyzer RSA II. Sample bars with dimensions 0.5 mm × 6 mm × 50 mm were tested in a dual cantilever beam arrangement. The tests were run with 0.2% strain at a frequency of 1 Hz and a temperature sweep from 25°C to 125°C. The temperature steps were 4°C and the soak time for each step was 120 s. The storage and loss modulus as well as $\tan \delta$ were logged. Three samples were analyzed for each withdrawal.

Dry Samples. It was revealed that the thin sheet samples lost a considerable amount of moisture during the relative short time it took to perform the mechanical tests. Therefore, after aging in water at 120°C samples were left drying for 48 h in desiccator to ensure consistent conditions of the samples during testing. All dried samples used for DMTA testing were aged more than 7 days to make sure that effects of plasticizer extraction were minimized.

RESULTS AND DISCUSSION

The results for density, weight loss, plasticizer extraction, molecular weight, tensile test, and DMTA are presented below. Note that the weight loss, density, TGA and initial DMTA test were performed on water saturated samples, while the tensile and rheological tests, as well as second DMTA test were run on dry conditioned samples. The purpose of the study was to investigate the link between changes in the mechanical properties and morphology of PA11 as the material degraded.

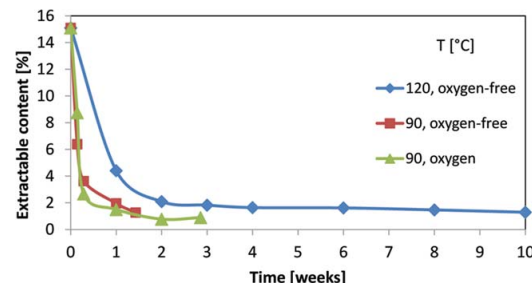


Figure 1. Plasticizer content for samples aged in 90°C and 120°C in both regular (TGA analyzed) and oxygen-free environment (vacuum oven analyzed). [Color figure can be viewed in the online issue, which is available at wileyonlinelibrary.com.]

Structure Characterization

Plasticizer Extraction and Water Saturation. Plasticizer is designed to soften the material, thus its depletion has a stiffening effect. Water is known to act in similar way to plasticizer, thus its absorption should have a softening effect.¹⁷

Volatile content analysis was performed for samples aged in 90°C and 120°C in both oxygen-free (vacuum oven/gravimetric analyzed) and oxygen-containing (TGA analyzed) environment. Figure 1 features the plasticizer extraction.

It can be seen that the rate of extraction is higher and residual plasticizer content lower for exposure at lower temperature. From purely kinetic point of view the opposite should be true, however above 95°C crystalline phase transitions occur in PA11 and crystallites gradually change from triclinic α to different hexagonal (γ , δ , and δ') forms.¹⁸ This structural change may be instrumental for plasticizer extraction behavior.

At 90°C most of the plasticizer is depleted during the first two days of exposure. After about 2 weeks for both temperatures extractable content stabilizes and amounts to just under 2% at 120°C and 1% at 90°C. From that point further property changes can be mainly ascribed to morphological changes. Oxygen does not seem to contribute significantly to the extraction rate.

Water content remaining in samples after each exposure time is featured in Figure 2. Values here are very low compared to the saturation level of 3% as stated in Rilsan documentation.³ The reason for this discrepancy is most likely water desorption from the samples while they have been stored and transported after exposures.¹⁷ Such situation occurs also in dry conditioned samples making the effect of water content on mechanical properties negligible. In order to assess this effect for saturated samples the water uptake curve has been estimated from TGA water loss and reported desorption levels. The exact procedure is described in the technical appendix— Supporting Information eqs. (S1) and (S2) and its result is featured in Figure 3.

The analysis indicates the presence of large initial moisture content. Observed postsaturation water content drop ($\approx 0.5\%$) is described in the literature and associated with the extraction of additives from soluble materials present in the matrix.¹⁷

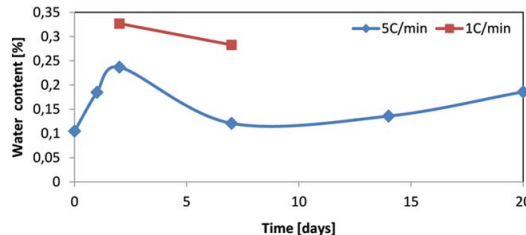


Figure 2. Water mass loss as measured with TGA at two heating rates for samples aged in 90°C. [Color figure can be viewed in the online issue, which is available at wileyonlinelibrary.com.]

Molecular Weight Evolution. Hydrolysis causes chain scissions contributing to lowering molecular weight and softening of the amorphous phase as well as its embrittlement.

Figure 4 features the comparison between measured number-average molecular weight and Jacques model predictions for exposures in 90°C and 120°C in oxygen-free water. CIV of the reference sample has been measured as 1.97 dL/g, which is equivalent to the number-average molecular weight of 40.64 kg/mol. For 90°, the prediction is fairly good for the first week of exposure. The result for 10 days is somewhat off, but it must be kept in mind that this data consist of single measurements only. The prediction for 120° is very good both regarding hydrolysis rate and position of equilibrium ($M_n = 17.33$ kg/mol or about 1.2 dL/g).

In addition some samples were also exposed to oxygen-containing water for 20 days. They showed no visible level of discoloration indicating only minor effects of parallel chain-scission mechanism of oxidation.

Crystallinity Ratio. Chain scissions destroy the entanglement network in the amorphous phase and liberate small molecular segments which can rearrange locally and initiate chemicrystallization.⁸ Crystallites contribute to stiffening of the material.

Crystallinity changes in aged samples were determined with DSC analysis. The degree of crystallinity was 21.7% for the reference sample. Since DSC tests were performed only on samples

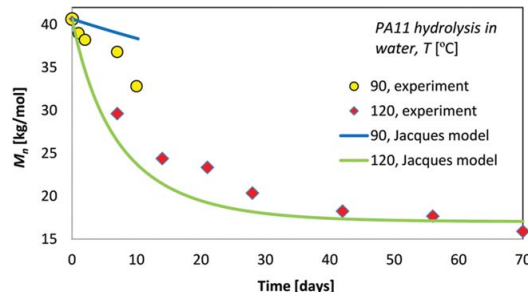


Figure 4. Experimental molecular weight evolution for samples aged in 90°C and 120°C and its prediction with Jacques model. [Color figure can be viewed in the online issue, which is available at wileyonlinelibrary.com.]

aged up to about 2 weeks, a different procedure was used to track crystallinity up to 10 weeks of exposure.

Crystallinity changes in samples aged more than 2 weeks (plasticizer effect minimized) were determined from density measurements. Densities of crystalline and amorphous phase were found to be 1.25 g/cm³ and 0.95 g/cm³, respectively, as calculated from eq. (5). Both were established from experimental sample density after 2 weeks and crystallinity χ at the same time from DSC analysis (at a slightly different exposure mode though).

A simple mixing rule for the density of the composite was utilized:

$$\varphi_{2w} = \varphi_c * \chi_{2w} * \varphi_a (1 - \chi_{2w}); \varphi_c > \varphi_a \quad (5)$$

where φ_{2w} and χ_{2w} are experimental sample density and crystallinity after 2 weeks of aging, respectively; φ_c , φ_a are fitted values for crystalline and amorphous density (assumed constant). Finally the degree of crystallinity as a function of time was calculated from the density evolution:

$$\chi(t) = \frac{\varphi(t) - \varphi_a}{\varphi_c - \varphi_a} \quad (6)$$

Each point is an average of three parallels.

Figure 5 shows the crystallinity changes as measured with both DSC and density measurements.

Property Characterization

Density Evolution. The curve obtained for the density as a function of time is shown in Figure 6. During the first 2 weeks of exposure plasticizer is being extracted resulting in an initial density drop. Then the density increases with the higher degree of crystallinity to finally stabilize on a plateau. The ultimate density is close to the initial one.

At all times the density remains higher than 1 g/cm³, therefore the material sinks in water.

CIV-Based Fracture Toughness. The CIV we obtained at equilibrium of long-term degradation is equivalent to the PA11 service acceptance criterion of 1.2 dL/g as in the API standard.¹ Therefore, samples aged for extended periods in high temperature water may risk undergoing ductile–brittle transition and

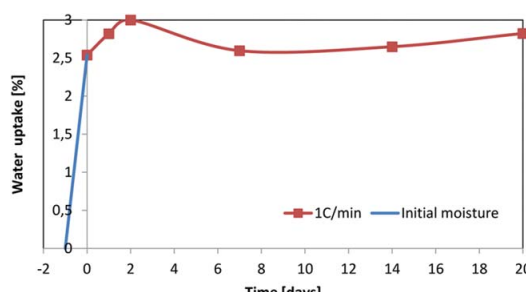


Figure 3. Water uptake estimate during aging in 90°C. It was obtained from measured water loss after accounting for desorption. [Color figure can be viewed in the online issue, which is available at wileyonlinelibrary.com.]

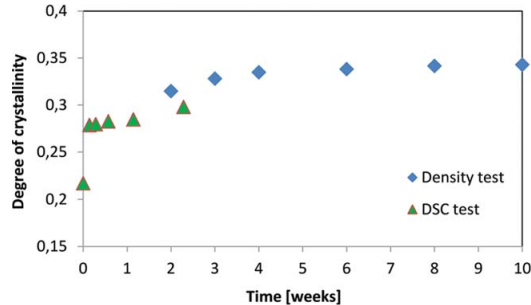


Figure 5. Crystallinity evolution of samples aged in 120°C as determined with DSC and density tests. [Color figure can be viewed in the online issue, which is available at wileyonlinelibrary.com.]

reduced elongation at break. However, at the same time CIV is far above the experience based failure criterion of 1.05 dL/g, so it is not certain whether embrittlement will happen.¹ The obtained CIV together with the industry experience indicate that elongation at break should still be greater than 200% and fracture toughness K_{IC} only marginally lower than 3 MPa m^{1/2} in most cases of long-term hydrolytic degradation.^{1,19} Therefore, occurrence of brittle failure must typically involve additional mechanisms of chain scission, e.g., oxidation or UV exposure.

Tensile Test. From the stress-strain curves in Figure 7 it can be seen that the compliant behavior of the virgin reference material ceases already after 1 week of aging. In the same period of time the material shows a prominent increase in the secant modulus and tensile strength, as displayed in Figure 8.

The average secant modulus data indicate a sharp stiffness increase between forth and sixth week of exposure, nevertheless further Dynamic Mechanical Analysis ruled out that outcome.

The tangential modulus taken at different strain levels for samples aged 1 and 10 weeks is featured in Figure 9. This quantity provides more precise information of the mechanical behavior in case of polymers exhibiting nonlinear characteristic already at very low strains.²⁰

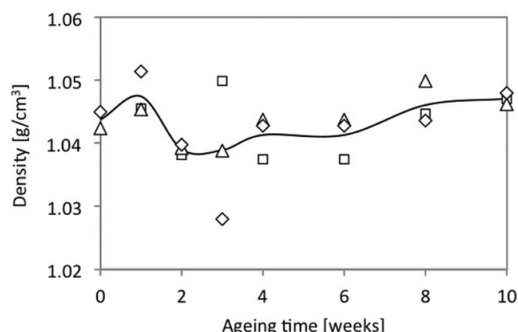


Figure 6. The density of PA11 during aging in water at 120°C. The different indicators represent the density of three individual samples and the line is the mean value at the given aging time.

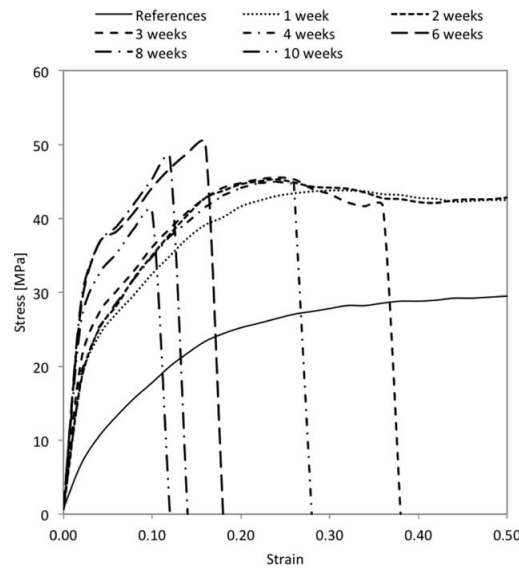


Figure 7. Stress-strain plots for PA11 aged in water at 120°C for up to 10 weeks.

The large initial increase in mechanical strength and modulus was expected due to the rapid initial dissociation of plasticizer. On the other hand a reduction of strength and modulus was

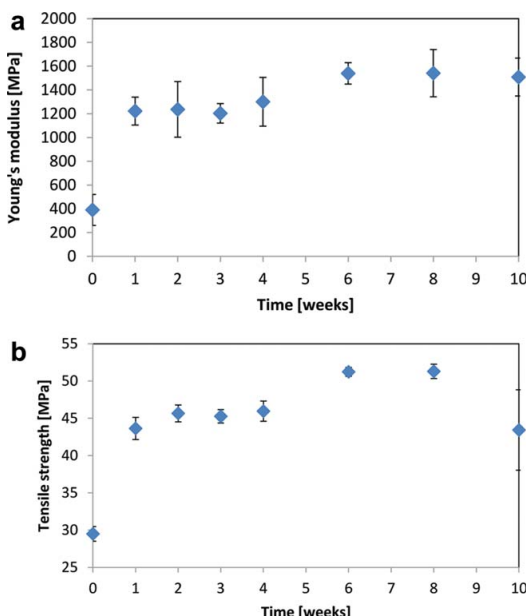


Figure 8. Young's modulus (0.2–0.5%) and tensile strength of PA11 aged in water at 120°C. Error bars represent one standard deviation from parallel values for each exposure time. [Color figure can be viewed in the online issue, which is available at wileyonlinelibrary.com.]

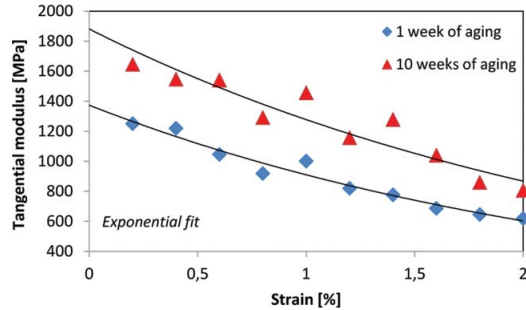


Figure 9. Tensile tangential modulus at different strain levels for 1 and 10 weeks exposures. [Color figure can be viewed in the online issue, which is available at wileyonlinelibrary.com.]

also expected from the big initial decrease in molecular weight as in Figure 5. This reduction was not observed. Apparently, the increase in mechanical properties due to reduced plasticizer content hid the possible decrease in properties caused by reduced molecular weight.

Dynamic Mechanical Thermal Analysis. The stiffness of the material is represented by its complex modulus as calculated with the formula:

$$E^* = \sqrt{(E^I)^2 + (E^{II})^2} \quad (7)$$

where E^I is the storage modulus and E^{II} is the loss modulus.

Damping efficiency is represented by loss tangent as calculated with the formula:

$$\tan \delta = \frac{E^{II}}{E^I} \quad (8)$$

Temperature dependence of dynamic mechanical properties. Figures 10 and 11 feature storage modulus and loss tangent of samples at different stages in degradation as a function of temperature. For all aging times the storage modulus decreases monotonically with temperature, while the loss modulus and loss tangent first reach a maximum. The peak value of $\tan \delta$ curve marks the glass transition temperature of the material.

Aging time dependence of dynamic mechanical properties. In general stiffness (represented here by storage modulus since effect of loss modulus is negligible) increases with aging time for all temperatures. This involves a better ability to store energy during deformation.

Dry samples aged for 4 and 6 weeks deviate from this rule, but it was found that they contained one strongly aberrant withdrawal each, making this data questionable.

At room temperature the storage modulus of the saturated samples increased with almost 200% during the first 2 weeks, largely because of plasticizer depletion. The increase rate declined for longer aging times.

The development of the storage modulus for saturated samples at room temperature as a function of aging time is shown in

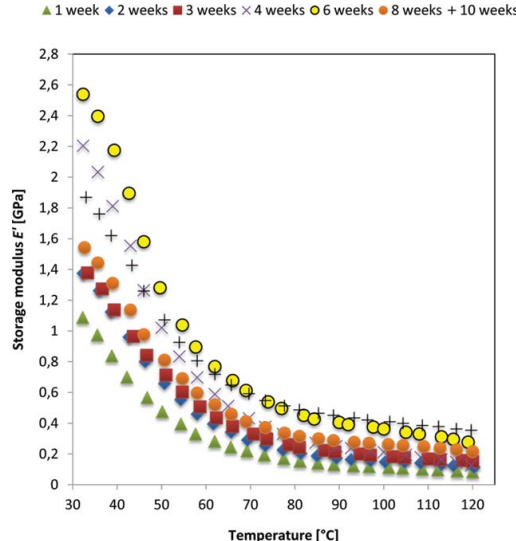


Figure 10. Storage modulus with temperature of PA11 samples aged in 120°C for 1–10 weeks and dry conditioned subsequently. [Color figure can be viewed in the online issue, which is available at wileyonlinelibrary.com.]

Figure 12. The trend was reproduced for higher temperatures, but the shifts were less remarkable.

Figure 13 features the storage modulus change with aging time at 30°C with error bars as well as mere averages for some other temperatures (this data showed much less variation).

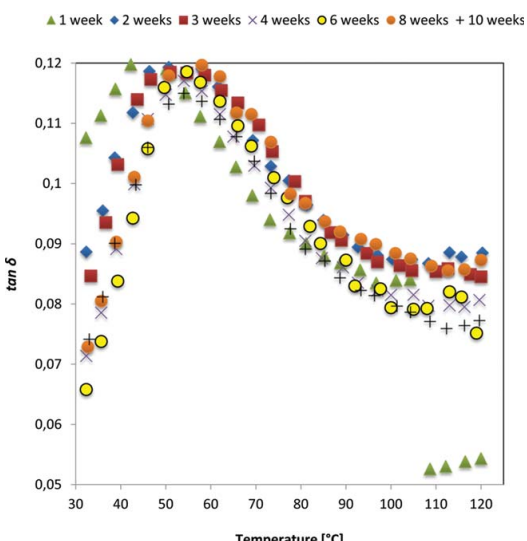


Figure 11. Loss tangent with temperature of PA11 samples aged in 120°C for 1–10 weeks and dry conditioned subsequently. [Color figure can be viewed in the online issue, which is available at wileyonlinelibrary.com.]

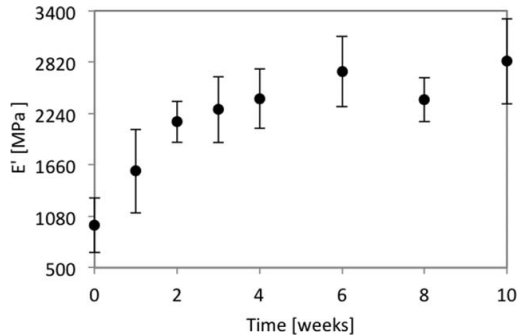
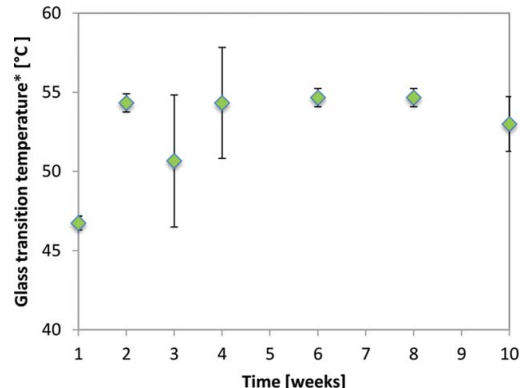


Figure 12. Storage modulus for saturated samples at room temperature as a function of aging time.

The experimental data was statistically corrected by removing some outliers with the procedure described in the technical appendix (Supporting Information Fig. S1.)

It is clear, that for higher temperatures (as well as for previously tested dry samples) the modulus increases with time to finally settle down on a plateau region. It can be similarly interpreted for 30°C as indicated by the trendline. This change in modulus with time confirms the validity of competing mechanisms: degradation creating low MW species decreasing the modulus and crystallization of low MW species increasing the modulus. It also largely rules out the occurrence of a previously considered sharp modulus increase after 4 weeks of exposure. A similar trend with aging time and temperature was observed for the loss modulus. Damping efficiency (represented by the loss tangent) seems to be affected negatively by the degradation for



* Estimated from maximum point of $\tan \delta$ curve at 1 Hz

Figure 14. Glass transition temperature for dry samples as a function of aging time. Error bars represent one standard deviation. [Color figure can be viewed in the online issue, which is available at wileyonlinelibrary.com.]

samples in the glassy state. The reduction of loss tangent was however not reproduced after samples have reached the glass transition temperature.

Aging time dependence of glass transition temperature. Modulus shifts along the temperature axis imply that the glass transition temperature T_g increases as the material ages. DMTA allows estimating the glass transition temperature as a function of time as shown in Figure 14. It can be clearly seen, that the glass transition temperature first rapidly increases and then after 2 weeks reaches a plateau region. T_g in this region ranges between 51°C and 55°C.

According to Fox and Flory²¹ the T_g of amorphous phase should decrease as the degradation proceeded and the molecular weight decreased. However, if the lower molecular weight products from the chain scission do not diffuse out of the material structure, but distribute in the polymer matrix, they will reorganize and cause a higher degree of crystallinity.⁸

A possible explanation and hypothesis in the present study is the T_g increase caused by immobile crystallites constraining amorphous chain segments, which now need higher energy input to get mobility levels of rubbery state. A previous study on aging of PA11 established the presence of lower molecular weight products in the polymer matrix by DSC measurements and the present study already confirmed the increase in crystallinity with aging time.⁹

Comparison between saturated and dried samples. Saturated samples are routinely stiffer than dried ones, which seems to be contrary to previous experience and theory. It means that either some important effects have been overlooked or more likely, that the DMTA apparatus has produced unknown sort of systematic error.

Figure 15 features a similar comparison with regard to glass transition temperature. It can be concluded, that the presence of water decreases the glass transition temperature. The plateau

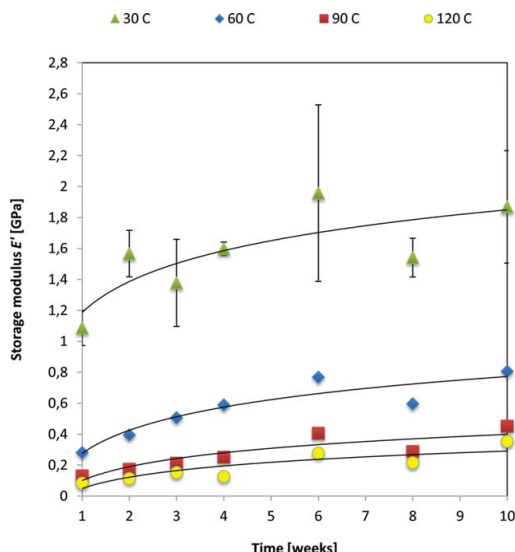


Figure 13. Storage modulus for dry samples at different temperatures as a function of aging time. [Color figure can be viewed in the online issue, which is available at wileyonlinelibrary.com.]

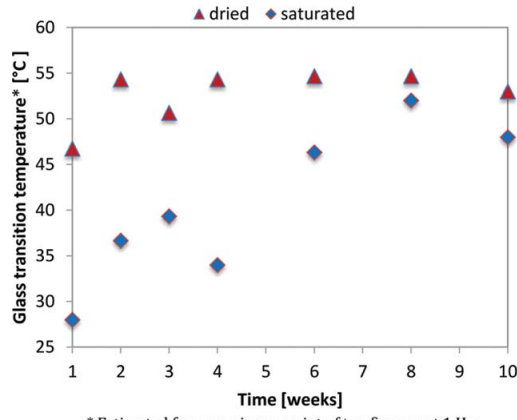


Figure 15. Glass transition temperature for dry and saturated samples as a function of aging time. [Color figure can be viewed in the online issue, which is available at wileyonlinelibrary.com.]

for saturated samples is reached much later in the degradation process, however it has similar value. This would indicate that water has been largely extracted by the eighth week of exposure.

Comparing Figures 11 and 16 allows concluding that saturation with water generally decreases damping efficiency of the PA11.

Property Evolution. Figure 17 features a general scheme of stiffness evolution with aging time for thin sheet PA11. After

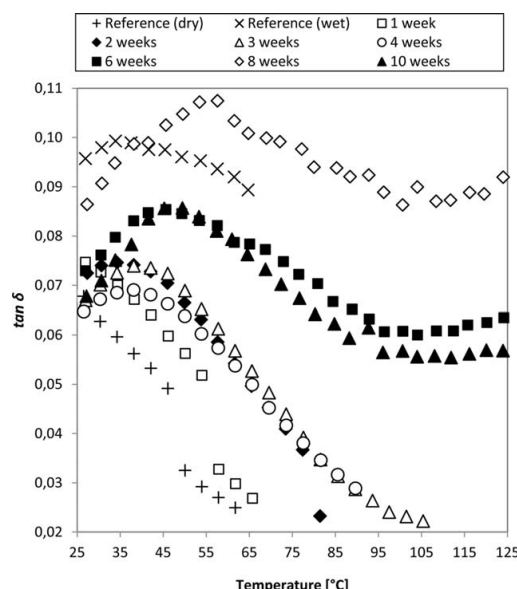


Figure 16. The $\tan \delta$ in flexure for PA11 aged for different periods in deoxygenated water at 120°C. The analyses were performed on samples saturated with water. Each point in the scatter represents the mean of three samples.

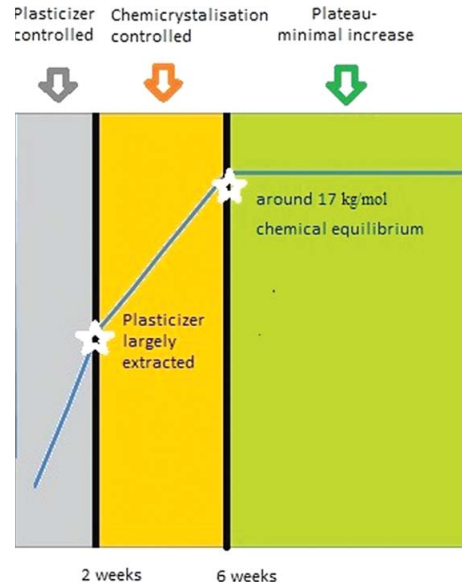


Figure 17. General scheme of PA11 stiffness evolution with aging time (thin sheet samples). [Color figure can be viewed in the online issue, which is available at wileyonlinelibrary.com.]

analyzing experimental data three distinct control domains have been identified:

1. *Plasticizer control.* With exception of the very initial period (first 1–2 days, sample getting saturated with water) stiffness increases following plasticizer extraction. Difference in modulus of over 1 GPa between plasticized and unplasticized PA11 grade is reported in the product specification.³ Therefore, effects of plasticizer extraction dominate over 10% crystallinity increase in the early stage of degradation. Most of the plasticizer is already depleted after a few days and after 2 weeks effects of further extraction should be negligible.

2. *Chemicrystallization control.* Plasticizer extraction and water saturation already came to their full effect in the previous phase, leaving chain scission induced softening of the amorphous phase and crystallization of the lower molecular weight products as the two governing mechanisms for stiffness evolution. Experiments showed that for the following month the modulus continues to increase with lower pace indicating that the stiffening effect due to crystallinity increase dominates here over continuous softening of the amorphous phase. The magnitude of this domination diminishes with time as degradation and chemicrystallization slow down.

3. *Plateau region.* After about 6 weeks into exposure the molecular weight gets asymptotically close to 17 kg/mol—equilibrium between hydrolysis and repolymerization. The modulus will continue to increase at an infinitesimal level thus essentially staying constant—this is the limit of water induced degradation. The change in the material structure in the aging periods based on stiffness evolution is shown in Table I. The mechanical and

Table I. PA11 Structural Parameters Evolution Dynamics with Aging Time

Aging time (weeks)	Plasticizer content	Crystallinity ratio	Molecular weight
0-2	↓	↑	↗
2-6	-	↙	↗
6-∞	-	-	-

volumetric properties can be expressed in an equivalent way, as shown in Table II. They can be seen as different functions of the three structural parameters from Table I. All these quantities are mutually interconnected thus it is possible to break their variability into similar time periods. This interconnection is strongly pronounced after 6 weeks of aging when all properties and structural parameters tend to reach a plateau.

Observing changes in the microstructure in detail, e.g., with an SEM, would provide parameters like crystallite size, shape, and orientation to supplement the information given by degree of crystallinity. Such studies should be performed in the future to improve the understanding of the underlying phenomena and the model predictions.

Thick samples. Based on the above it is also possible to estimate stiffness evolution of real life thick samples. Plasticizer molecules are relatively large and it would take a long time for them to diffuse out of a thick liner. Slow removal of the plasticizer would cause a slow gradual increase in modulus over the years. In short term this increase would not be significant. Since diffusion of water is very fast in polyamides²² chemicrystallization would control stiffness increase for the first 6 weeks. Then the degree of crystallinity reaches plateau, but plasticizer continues to be slowly extracted. The modulus continues its slow gradual increase and is now controlled by plasticizer extraction. Therefore, for thick samples, stiffness plateau is reached after several years, once the plasticizer is completely diffused out.

CONCLUSIONS

There are four main mechanisms of property change. Plasticizer extraction contributes to stiffening of the material (modulus and strength increase), T_g increase and density decrease—partially diminished by water absorption acting as plasticizer. Moreover hydrolysis has a dualistic effect on properties: chain scissions destroy the entanglement network in the amorphous phase (softening, embrittlement, T_g decrease) and liberate small molecular segments which rearrange locally and initiate chemicrystallization (stiffening, T_g and density increase).

Table II. PA11 Property Evolution Dynamics with Aging Time

Aging time (weeks)	Modulus	Strength	T_g	Density
0-2	↑	↑	↑	↗
2-6	↙	↙	-	↙
6-∞	-	-	-	-

Experimental results regarding changes in morphology and properties of PA11 under hydrolytic degradation in 120°C have been compared and the main findings are listed as follows:

- Occurrence of brittle failure by hydrolysis only is rare and typically involves additional mechanisms of chain scission, e.g., oxidation or UV exposure
- Mechanical properties evolution can be divided into three control domains for thin PA11 materials:
 1. *Plasticizer control*—first 2 weeks, stiffness and strength—rapid increase
 2. *Chemicalcrystallization control*—following month, stiffness, and strength—moderate increase
 3. *Plateau region*—after about 6 weeks, stiffness, and strength—infinitesimal increase
- The glass transition temperature increases as the degradation proceeds—contrary to Fox and Flory theory for amorphous regions. It can be explained by the fact, that amorphous chain segments get constrained by the immobile crystallites following chemicalcrystallization

Moreover interesting supporting findings have been listed below:

- PA11 sinks in water at all aging times. The ultimate density is close to the initial one
- Damping efficiency (loss tangent) is affected negatively by degradation for samples in the glassy state, but not in rubbery state
- Presence of water contributes to the decrease in both glass transition temperature and damping efficiency

This work investigated the link between mechanical behavior and morphology of PA11 during degradation through tensile testing, DMTA and material characterization techniques. Experimental results obtained here will be compared with a multiscale model for PA11 hydrolytic degradation in another article (Part 2). Fatigue behavior and some additional analysis should also be detailed elsewhere.

ACKNOWLEDGMENTS

This work is a part of the “PolyLife” project managed by SINTEF Materials and Chemistry. The authors would like to express their gratitude for the financial support by the Norwegian Research Council (grant 193167).

REFERENCES

1. API TECHNICAL REPORT 17TR2, The Ageing of PA 11 in Flexible Pipes, API Publishing Services: Washington, DC, **2003**.
2. API RECOMMENDED PRACTICE 17B, Recommended Practice for Flexible Pipe, API Publishing Services: Washington, DC, **2008**.
3. Rilsan® PA11: Created From a Renewable Source; Arkema: France, **2012**.
4. Boschee, P. *Oil Gas Facil.* **2012**, *15*.
5. Groves, S. Ed. 20th International Conference on Offshore Mechanics and Arctic Engineering, Rio de Janeiro, Brazil, ASME: **2001**.

6. Meyer, A.; Jones, N.; Lin, Y.; Kranbuehl, D. *Macromolecules* **2002**, *35*, 2784.
7. Jacques, B.; Werth, M.; Merdas, I.; Thominette, F.; Verdu, J. *Polymer* **2002**, *43*, 6439.
8. El-Mazry, C.; Correc, O.; Colin, X. *Polym. Degrad. Stab.* **2012**, *97*, 1049.
9. Romao, W.; Castro, E. V. R.; Filho, E. A. S.; Guimaraes, R. C. L.; Silva, A. L. N.; Teixeira, S. C. S. *J. Appl. Polym. Sci.* **2009**, *114*, 1777.
10. Domingos, E.; Pereira, T. M. C.; Castro, E. V. R.; Guimaraes, R. C. L.; Romao, W. *X-Ray Spectrom.* **2013**, *42*, 79.
11. Pinel, E.; Mason, J.; O'Brien, G. NACE International Meeting, Corrosion Proceedings—Paper #04713, March, New Orleans, USA, **2004**.
12. Mazan, T.; Berggren, R.; Jørgensen, J. K.; Echtermeyer, A. T. *J. Appl. Polym. Sci.* to be submitted for publication.
13. ASTM D792-08, Standard Test Methods for Density and Specific Gravity (Relative Density) of Plastics by Displacement, ASTM, USA, **2008**.
14. Schnabel, W. Aspects of Degradation and Stabilisation of Polymers; Elsevier: Amsterdam, **1978**; Chapter 4, p 149.
15. Sichina, W. J. DSC as Problem Solving Tool: Measurement of Percent Crystallinity of Thermoplastics. PETech-40 Thermal Analysis, PerkinElmer, **2000**.
16. Ying, S.; Lin, Y.; Tao, Y. *J. Appl. Polym. Sci.* **2008**, *110*, 945.
17. Silva, L.; Tognana, S.; Salgueiro, W. *Polym. Test.* **2013**, *32*, 158.
18. Zhu, J.; Zhang, X. Y.; He, B. 12th International Symposium on Electrets, September 11–14, Bahia, Brazil, **2005**.
19. Berger, J. The Compatibility and Aging of Polyamides With Production Fluids. EVONIK industries, MERL Oilfield Engineering With Polymers Conference, October 23–25, London, UK, **2012**.
20. Echtermeyer, A. T. Proceedings of 2nd European Conference on Composites Testing & Standardisation, September 13–15, Hamburg, Germany, **1994**.
21. Fox, T. G.; Flory, P. J. *J. Appl. Phys.* **1950**, *21*, 581.
22. Wu, P.; Siesler, H. W. *Chem. Mater.* **2003**, *15*, 2752.

PAPER B

Tobiasz Mazan, Jens Kjær Jørgensen and Andreas Echtermeyer

Aging of Polyamide 11. Part 2: General multiscale model of the hydrolytic degradation applied to predict the morphology evolution

Journal of Applied Polymer Science, Volume 132, Issue 41, pages 12039-12049; Aug 4, 2015

Aging of polyamide 11. Part 2: General multiscale model of the hydrolytic degradation applied to predict the morphology evolution

Tobiasz Mazan,¹ Jens Kjær Jørgensen,² Andreas Echtermeyer¹

¹Department of Engineering Design and Materials, Norwegian University of Science and Technology, Trondheim 7034, Norway

²SINTEF Materials and Chemistry, Oslo 0373, Norway

Correspondence to: T. Mazan (E-mail: tobiasz.mazan@ntnu.no)

ABSTRACT: Accelerated aging tests are the conventional way to evaluate long-term degradation of polymers, in particular for offshore flexible risers. In this article, a multiscale model has been developed combining diffusion, chemical kinetic reactions, structure–property relationships, and composite models to provide faster and less labor extensive property predictions. A general methodology is presented and applied to predict the density and crystallinity evolution. Results are compared with experimental ageing of polyamide 11 in deoxygenated water at 120°C. For both density and degree of crystallinity the modeled trend is close to the experimental test results. Accurate prediction of the morphological parameters during degradation allows extension of the multiscale model for the prediction of mechanical properties. © 2015 Wiley Periodicals, Inc. *J. Appl. Polym. Sci.* **2015**, 132, 42630

KEYWORDS: crystallization; degradation; oil & gas; polyamides; theory and modeling

Received 11 March 2015; accepted 18 June 2015

DOI: 10.1002/app.42630

INTRODUCTION

Polymeric materials find many applications in the offshore oil and gas industry with special emphasis on sealing and piping elements. In both cases unexpected failure can lead to significant economic and environmental hazards, which makes the understanding of long-term degradation mechanisms of key importance.¹ Absorption and diffusion of fluids, as well as the chemical reactions they can promote, are already well understood; nevertheless, the link between molecular effects and macroscopic material properties is still largely missing. Therefore, long term performance under chemical and mechanical factors is evaluated totally by long-term testing in the expected environment (typically a month to a year) and statistical extrapolation of the results to lifetimes of 20–50 years without understanding of science behind degradation phenomena.² This approach can serve industry pretty well under the assumption, that all degradation modes occurring in the material have been exposed in full prominence during test time. However, reality is often different and actual failure may happen long before (or after) the expected one.³ Accelerated tests are often performed, but they require increased temperature and as such cannot be used for materials with a low melting point. Moreover both regular and accelerated tests are valid only for materials of a certain morphology exposed to a certain environment. Without understanding how each factor (and their interplay) affects global properties extrapolation of results to different cases is difficult. Very often even trace elements in an

environment or slight differences in polymer microstructure can lead to significant changes in degradation over time.⁴ Summarizing, currently used empirical–statistical approaches for predicting long term environmental degradation not only require very long testing times but also results, which can be obtained, are often far from being accurate.² Therefore, faster and more reliable evaluation methods are needed. The bottom-up multiscale approach is proposed here as a good way to address this problem. It is divided into four fundamental stages:

- Evaluation of the environmental agents (water, oxygen, acids, etc.) concentration profile in the polymer with time,
- Effect of chemical action of the environmental agent on the polymer molecular properties with time,
- Microstructure–property relationship yielding local mechanical properties of the polymer,
- Combining the local properties into global material properties.

This article as Part 2 of a series describes the details of the model and compares predictions against the morphology data: density and crystallinity. The experiments were shown in Part 1.⁵ The model can also be expanded further to describe stiffness and strength. This aspect will be presented in Part 3.⁶

GENERAL MULTISCALE MODEL FOR DEGRADATION

There are numerous models concerning each separate stage of the presented method, however a holistic approach combining

them into a multiscale model has been missing. The aim of this work is to address this issue by developing a model linking chemical degradation on the microscale to macroscopic properties of the material. The approach is described first in general terms and then more specifically for Polyamide 11.

The general stages outlined here are shown in Figure 1. They will be applied for a specific case: the hydrolytic degradation of PA11. Two specific quantities will be addressed in the later parts of this article:

- Density
- Degree of crystallinity

Moreover the following properties will be considered in the succeeding paper:⁶

- Young's modulus
- Tensile strength
- Embrittlement threshold
- Mechanical equilibrium

The general approach suggested here for polymer properties prediction consists of four basic stages, as shown in Figure 1 and described in the following paragraphs.

Stage 1: Concentration Profile

The first stage is to calculate the concentration profile of the environmental agent in the selected material over time. To do so a certain diffusion model must be chosen and the model's constants need to be measured. Typically Fick's diffusion model is chosen, but if the shape of the concentration profiles is critical the validity of the model should be checked.

The concentration profile can be found by exploring literature resources or by performing tests on thin films. In the simplest case, diffusion parameters for different substances are treated as independent factors with possible model adjustment for their interplay. Basically two types of experiments are used to find both diffusivity and solubility of the material. In the first one, a flat plate (or thin film to safe time) is exposed on both sides to the solute and then the weight uptake as a function of time is recorded. There, initial rate of weight uptake is a function of diffusivity and terminal weight uptake is the solubility. In the other experiment, exposure is only one-sided and the amount of permeate going through the sample is measured.

Stage 2: Kinetic Model—Molecular Level

In the second stage, the local molecular structural changes with time are evaluated as a result of a certain concentration of reactive agent. This is a crucial part of the methodology as it predicts the molecular response in the long-term perspective, which cannot be encompassed empirically. The most important property changes addressed in this task are chemical (kinetic) reactions, swelling, and degree of crystallinity. A result of chemical reactions is typically chain scission resulting in a molecular weight decrease in the amorphous phase. For semicrystalline polymers, the molecular weight decrease is often followed by an increased ratio of crystalline phase, because the low molecular weight components can crystallize easily.⁷ The most important

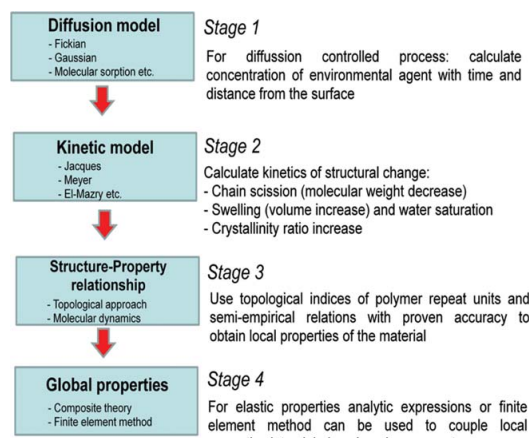


Figure 1. General scheme showing the stages of multiscale modeling of polymers. [Color figure can be viewed in the online issue, which is available at wileyonlinelibrary.com.]

reactions will have to be identified along with at least some respective rate constants and species concentrations. Then kinetics of the microstructural change can be expressed in terms of kinetics of individual reactions. This would often require solving adequate differential equation system.⁸ If reactions occur very quickly time dependence can be skipped and experimental structural change can be used directly.

Scale Bridging: Stage 2 to Stage 3

Individual models are designed to operate on quantities in certain scale ranging from subatomic calculation to design of large engineering structures. Sometimes it is possible to directly use output parameters from smaller scale model as an input for larger scale models. Most of the time, however, a scale bridging procedure is needed to integrate single-scale models and create larger multiscale model.

In the case of the multiscale model of degradation proposed here only one scale bridging procedure must be used. The kinetic model in stage 2 provides molecular weight of the aged material, while formulas in stage 3 are functions of monomer topology and glass transition temperature.

Therefore, the dependence of the glass transition temperature on molecular weight $T_g(M_n)$ should be obtained.) $T_g(M_n)$ can be found by using the Fox and Flory equation:^{9,10}

$$T_g(M_n) \approx T_g^\infty - 0.002715 \frac{(T_g^\infty)^3}{M_n} \quad (1)$$

where T_g^∞ is the hypothetical T_g for infinite molecular mass. T_g^∞ is a material specific parameter and can be obtained by assuming an initial T_g for a specified M_n and solving the former equation.

Stage 3: Structure–Property Relationship

Topological Approach. In the third stage, local mechanical properties are to be evaluated as a result of structural changes in the polymer. To do so, we will mainly use topological

formalism using connectivity indices defined via graph theoretical concepts as its main descriptors. Topology is simply the pattern of interconnections between atoms in a polymer repeat unit and connectivity indices contain information on electronic configuration and coordination number for each one of them.⁹ Correlating these parameters with experimental data enables to quantitatively predict polymer properties from given structural information. It is typically done by expressing fundamental material properties (volume occupied by the molecule, cohesive energy, etc.) as a function of topology and combining them into derived properties (such as density or elastic constants).⁹ It has been shown, that all the additive properties can be expressed in terms of linear combinations of graph theoretical invariants, which constitutes a theoretical basis for the method.¹¹ The procedure is supported by many theoretical and semiempirical interrelations with proven accuracy, for example, dependence of glass transition temperature on molecular weight. Extensive databases containing such correlations are already available and can be expanded for new properties and polymers by performing experiments or group contribution calculations.⁹ This procedure has proven its robustness for practical cases many times.⁹

The topological approach by Bicerano has been chosen as a model for structure–property relationship in the amorphous phase.⁹ The crystalline phase is considered impenetrable for environmental agents and thus has constant properties during degradation.

Key Concepts of the Topological Method. Based on the literature a summary of the key concepts of the topological approach is given here:⁹

- Connectivity indices

Connectivity indices describe the topology (connectivity) of the monomer. They include two categories—primary and aggregate connectivity indices.

- Primary indices

The simple atomic connectivity index δ -describes the number of non-hydrogen atoms to which a given non hydrogen atom is bonded

The valence atomic connectivity index δ^V -gives information on details of the electronic configuration of each non-hydrogen atom:

$$\delta^V \equiv \frac{Z^V - N_H}{Z - Z^V - 1} \quad (2)$$

where is Z^V is a number of valence electrons of an atom, N_H is the number of hydrogen atoms bonded to an atom and Z is the atomic number of the atom.

Simple and valence bond connectivity indices β are the product of simple and valence atomic indices respectively on the vertices (i and j) defining a given bond:

$$\beta_{ij} = \delta_i * \delta_j \text{ and } \beta_{ij}^V = \delta_i^V * \delta_j^V \quad (3)$$

- Aggregate indices

Zeroth-order and first-order aggregate connectivity indices, X_0 , X_0^V , X_1 , X_1^V are summations of the reciprocal square roots of the primary connectivity indices over either vertices (atoms) or edges (bonds) of the monomer:

$$X_0 \equiv \sum_{\text{vertices}} \left(\frac{1}{\sqrt{\delta}} \right) \quad (4)$$

$$X_0^V \equiv \sum_{\text{vertices}} \left(\frac{1}{\sqrt{\delta^V}} \right) \quad (5)$$

$$X_1 \equiv \sum_{\text{edges}} \left(\frac{1}{\sqrt{\beta}} \right) \quad (6)$$

$$X_1^V \equiv \sum_{\text{edges}} \left(\frac{1}{\sqrt{\beta^V}} \right) \quad (7)$$

- Fundamental properties

Fundamental properties are properties in the microscale, for example, van der Waals volume, cohesive energy, and so on. They are correlated with aggregate connectivity indices X , structural parameters (e.g., number of rotational degrees of freedom), and correction terms N (e.g., number of amide groups) as descriptors of the polymer repeat unit using an equation of the general form given below:

$$\begin{aligned} \text{Microscale property} &= (\Sigma a X) + (\text{Structural Parameters}) \\ &+ (\text{Atomic and Group Correction Terms}) \end{aligned} \quad (8)$$

where a is a fit parameter.

A wide range of such combinations with different connectivity indices, structural parameters, correction terms, and fit parameters was obtained by Bicerano⁹ and the parameters giving the best fit to experimental or literature data were chosen to be included in his topological model.

- Derived properties

Derived properties are properties in the macroscale, for example, density, solubility, modulus. They can be expressed in terms of combinations of fundamental properties and thus indirectly relate to the topology of the monomer. Correlations developed by Seitz for mechanical properties are of key importance.^{9,12} It is a semiempirical approach in which experimental data is fitted with equations from thermodynamic and molecular theories.¹²

Alternative Methods. A number of alternative approaches may be used instead of the topological approach or as a supplement. Examples are the group contribution technique, experiments, and molecular dynamics. The group contribution technique provides quantitative structure–property relationships. This method considers contributions to a certain mechanical or thermodynamic property made by all chemical groups (such as $-\text{CH}_2-$ or $-\text{OH}$) constituting the polymer repeat unit.¹³ The main limitation of this technique is that a polymer property cannot be predicted if a value of a single group contribution cannot be estimated, which triggered development of the topological approach described above.⁹

Moreover, it is possible to use the experimental method, which would require preparation of samples with different molecular weights, densities, and phase ratios followed by mechanical testing. Such an experiment in conjunction with chemical modeling should allow formulating time dependent property profiles. Nevertheless, the usefulness of this approach is limited by the ability to control the microstructure of samples obtained, for

example, it is difficult to synthesize a set of samples differing in molecular weight with otherwise identical microstructure. Samples will always be varying in parameters like density, polydispersity, amount of contamination, and so on resulting in uncertainty regarding the exact effect of each structural feature.

Molecular dynamics is another method. It involves building a polymer structure model on an atomistic scale and performing subsequent computer simulations. This method can give interesting qualitative insights into the workings of polymer materials. However, due to time limitation and scale bridging issues, it should be probably treated as a last instance tool for the quantitative evaluation.^{14–16} Currently available computational power provides simulations on atomic level for not more than several nanoseconds.¹⁷ Also, coupling between atomistic level and mesoscale is specific to each system modeled and not straightforward.^{15,16}

Stage 4: Global Properties

The global effect of the local material degradation needs to be found. Materials containing a number of volume elements with different properties can be treated as composites. Various methods, such as Finite Element Analysis or composites theory, for example, Halpin,¹⁸ can be used to combine the varying properties into global engineering parameters.

MULTISCALE MODEL FOR HYDROLYTIC DEGRADATION OF POLYAMIDE 11

This section shows how the general multiscale approach can be applied to the case of Polyamide 11 degradation. Models operating on different scale-levels have been chosen for their demonstrated accuracy and ability to fit the multiscale model in a relatively straightforward manner—avoiding major scale bridging issues. While diffusion and structure–property models will be similar for most polymers and can be adjusted by using different input parameters, the kinetic model is specific to one process in one material. In our case it is hydrolytic chain scission in Polyamide 11.

Stage 1: Fast Saturation

In the case of PA11 exposed to water diffusion proceeds very fast and the environmental agent can be considered uniformly distributed within the material.¹⁹ Diffusion in polyamides is also generally assumed to follow Fick's law.²⁰

Figure 2 shows the modeled relative concentration of water with time in the centre of a 20-cm diameter PA11 element:

$$c_{\text{rel}} = \frac{c(x, t)}{c_0} \quad (9)$$

where $c(x, t)$ is the concentration at time t and distance x from the surface, c_0 is the concentration at a boundary located at position $x = 0$. The diffusion coefficient of water in Polyamide 11 was found in the literature.¹⁹ To estimate water concentration the 1D-Fick's law was used:²¹

$$c(x, t) = c_0 \operatorname{erfc} \left(\frac{x}{2\sqrt{Dt}} \right) \quad (10)$$

where erfc is the complementary error function approximated here by the first two terms of its Taylor series, $2\sqrt{Dt}$ is the diffusion length providing a measure of how far the concentration has propagated in the x -direction by diffusion in time t .

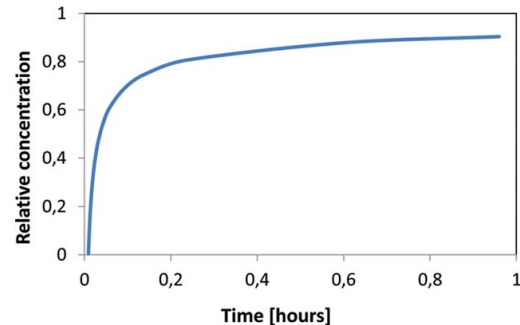


Figure 2. Modeled water concentration with time at distance $l/2 = 10$ cm from the surface, $D_{50^\circ\text{C}} = 9.91 \times 10^{-9} \text{ cm}^2/\text{sec}$, Fickian behavior assumed. [Color figure can be viewed in the online issue, which is available at wileyonlinelibrary.com.]

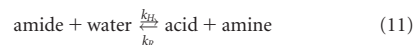
It can be seen that after just 1 h exposure the relative concentration reaches 90%. It takes several days before complete saturation of the material.

For the remaining parts of the article, it will be assumed that diffusion of water into the PA happens very quickly compared to the typical lifetimes of 25 years or more required in offshore applications. The PA11 material will be seen as completely saturated and Stage 1 will not be considered any further.

Stage 2: Jacques Kinetic Model

Jacques model has been chosen to evaluate the kinetics of hydrolytic chain-scission due to its relative simplicity and confirmed accuracy.²² A summary of this kinetic model is given in the following section.

The general governing reaction for PA11 hydrolysis is:²²



The reaction occurs in amorphous phase only as the crystalline regions are considered impenetrable to water.¹⁹

The number of chain scissions (mol/kg) at time t can be expressed as follows:

$$n = \frac{1}{M_n} - \frac{1}{M_{n0}} \quad (12)$$

$$n = [\text{Amide}]_0 - [\text{Amide}] = [\text{Acid}] - [\text{Acid}]_0 = [\text{Amine}] - [\text{Amine}]_0 \quad (13)$$

where M_n is the number-average molar mass and the subscript zero corresponds to the initial (virgin) state. The basic kinetic equation can thus be written as:²²

$$\begin{aligned} r(W) &= \frac{dn}{dt} = k_H[\text{Amide}][\text{Water}] - k_R[\text{Acid}][\text{Amine}] \\ &= k_H([\text{Amide}]_0 - n)[\text{Water}] - k_R([\text{Acid}]_0 + n)([\text{Amine}]_0 + n) \end{aligned} \quad (14)$$

where $r(W)$ is the rate of hydrolysis, k_H , k_R are the hydrolysis and recombination reaction constants.

Jacques model uses the following simplifications:²²

Table I. Constants of Jacques kinetic Model for Hydrolysis of PA11

Symbol	Name	Value	Unit
K_0	Rate constant at infinite temperature	7×10^{11}	1/day
E_k	$K(T)$ sensitivity factor ("activation energy")	97	kJ/mol
R	Universal gas constant	8.31	J/kg K
M_{ne0}	Equilibrium molecular weight at infinite temperature	2.36	kg/mol
E_m	$M_{ne}(T)$ sensitivity factor ("activation energy")	-6.46	kJ/mol
W_{s0}	water solubility at infinite temperature	1	mol/kg
E_w	$W_s(T)$ sensitivity factor ("activation energy")	4	kJ/mol
E_0	Initial amount of amide groups	5.46	mol/kg

- The amide conversion ratio at embrittlement is very small and can be neglected relatively to its initial concentration E_0
- Conditions of the polymerization process make initial acid concentration and initial amine concentration differ very little and are here assumed to be equal: $A_0 = B_0$

Experiments determined the quantities K (pseudo-rate constant) and M_{ne} (equilibrium molar mass) from which the basic rate constants k_R and k_H can be calculated:

$$k_R = \frac{KM_{ne}}{2} \quad \text{and} \quad k_H = \frac{k}{2M_{ne}[\text{Amide}]_0[\text{Water}]} \quad (15)$$

The temperature dependence of the rate constants (correlations for K and M_{ne}) and water solubility in the polymer is given by the Arrhenius law. Table I features all constants assumed in the Jacques model.²²

Finally an expression for $M_n(t)$ is obtained by integrating eq. (14) and combining the result with eq. (12):²²

$$M_n(t) = M_{ne} \frac{M_{n0}^{-1} + M_{ne}^{-1} + (M_{ne}^{-1} - M_{n0}^{-1}) \exp(-Kt)}{M_{n0}^{-1} + M_{ne}^{-1} - (M_{ne}^{-1} - M_{n0}^{-1}) \exp(-Kt)} \quad (16)$$

In this article, for the aging temperature $T = 120^\circ\text{C}$ and initial molecular weight⁵ $M_{n0} = 40.64 \text{ kg/mol}$, values of the rate constants are as follows: $k_R = 0.77$ and $k_H = 0.0017 \text{ kg/mol day}$.

Scale Bridging: $T_g(M_n)$ function

The Fox and Flory equation was used to obtain the $T_g(M_n)$ relationship as described previously. The result of this procedure for the studied PA11 sample (40.64 kg/mol^5 , $T_g = 318 \text{ K}^{23}$) is shown in Figure 3. The glass transition temperature drops by 18 K for 5 kg/mol and falls rapidly when the molecular weight drops below about 3 kg/mol.

Stage 3: Structure–Property Relationship

The architecture of the PA11 repeat unit (as given in Figure 4) was analyzed with eqs. (2–7) and the following values for connectivity indices of PA11 were obtained to be used in the model:⁹

$$X_0 = 9.3555 \quad (17)$$

$$X_0^V = 8.4793 \quad (18)$$

$$X_1 = 6.3938, \quad (19)$$

$$X_1^V = 5.6612 \quad (20)$$

The exact procedure of obtaining structure–property relationships in the Stage 3 depends on property to be calculated. It is described in detail for density and crystallinity in later parts of this article and for the mechanical properties in the following paper.⁶

Stage 4: Uniform Properties

In this article describing PA11, we have an even distribution of water through the body, since the diffusion happens very quickly. Moreover the current modeling approach assumed the sample to be perfectly homogenous. This means properties will be the same throughout the material and global engineering properties do not need to be calculated. Therefore, Stage 4 will not be considered further.

PREDICTION OF THE PA11 MORPHOLOGICAL PROPERTIES

This section contains detailed property prediction procedures for the degree of crystallinity and density evolution. It also features a comparison between model and experiment. An

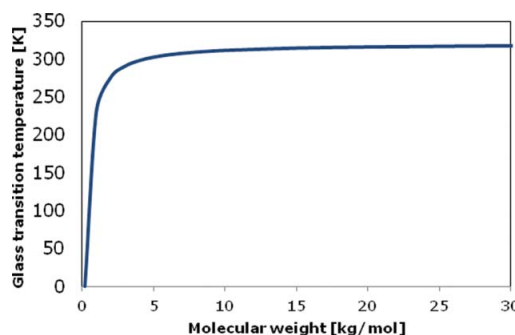


Figure 3. Glass transition temperature of amorphous PA11 as a function of molecular weight (Fox and Flory). [Color figure can be viewed in the online issue, which is available at wileyonlinelibrary.com.]

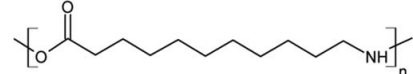


Figure 4. Molecular structure of the Polyamide 11 repeat unit. Empty vertices represent $-\text{CH}_2-$ group.

Table II. Constituent Models of the Multiscale Approach to Predicting Density and Crystallinity

Property modeled (multiscale approach)	Constituent models
Density	Jacques ²
	Fox and Flory ²⁻³
	Bicerano ²⁻³ topological
	Crystallinity multiscale ³
	Rule of mixtures ³
Crystallinity	Jacques ²
	Fox and Flory ²⁻²
	Bicerano ²⁻² topological
	Fayolle ²

Numbers indicate stage or scale bridging in which certain model was introduced, reference in the main text.

analogous section in Part 3 of this article series will consider Young's modulus, yield strength, brittleness, and mechanical equilibrium.⁶

Experimental results relevant for the modeling described here were reported in detail previously.⁵ They are sometimes reported with error bars to give a statistically meaningful comparison between model predictions and laboratory testing. The

error bars represent one standard deviation of parallel laboratory test results.

Input and Output Parameters

Table II lists the constituents of multiscale models applied here. Table III shows input parameters for these constituent models, their values to be used with PA11 property predictions along with reference and the output parameters produced by the model.

Input parameters can be generally divided into constants and variables. The constants are the parameters specific for a certain polymer system. The variables describe conditions specified by the application. Such variables include aging conditions (hydrolysis temperature and time) and initial parameters of the studied sample (initial molecular weight and degree of crystallinity).

The final output includes density and degree of crystallinity as functions of aging time as well as some intermediary parameters as listed in Table III.

Predicting Crystallinity

Chain scissions destroy the entanglement network in the amorphous phase and liberate small molecular segments which diffuse toward crystals surface and initiate chemicrystallisation.⁷ The Fayolle model predicts the degree of crystallinity during degradation as a function of initial crystallinity, molecular weight and entanglement molecular weight.⁷ To calculate

Table III. Input and Output Parameters of the Constituent Models in the Multiscale Approach

Model	Input parameters	Values chosen	Output parameters
Jacques	- T_{hyd} , hydrolysis temperature	120°C—slightly above riser working conditions ²³	$M_n(t)$ —number average molecular weight
	- M_{n0} , initial molecular weight	40.64 kg/mol—experiment ⁵ (part 1)	
	- t , hydrolysis time	Independent variable	
Fox and Flory	- T_g^{MW} , initial T_g for specified molecular weight	45°C for 40.64 kg/mol, literature ²³ T_g for M_{n0}	$T_g(M_n)$, glass transition temperature
	$M_n(t)$	Jacques model	
Bicerano topological	$T_g(M_n)$	Fox and Flory model	M_e , entanglement molecular mass; Φ_a , density of the amorphous phase
	Connectivity	$X_0 = 9.3555$, $X_0^V = 8.4793$, $X_1 = 6.3938$, $X_1^V = 5.6612$ from literature ⁹	
	- M , monomer mass	174.2 g/mol from literature ⁹	
Fayolle	- l_m , monomer length	14.05 Å, self-calculated from geometry of monomer	
	- T , test temperature	25°C, room temperature assumed	
	- X_{c0} , initial crystallinity ratio	21.7%, experiment ⁵ (part 1)	$-X_c(t)$, degree of crystallinity
	M_{n0} , $M_n(t)$	Jacques model	
Rule of mixtures (density)	M_e	Bicerano model	
	- Φ_a , density of the amorphous phase	0.94 g/cm ³ , Bicerano model	$-\Phi_{sc}(t)$, density of the semicrystalline polymer
	- Φ_c , density of the crystalline phase	1.25 g/cm ³ , experiment ⁵ (part 1)	
	$X_c(t)$	Fayolle model	

crystallinity change during hydrolysis of PA11 molecular weight was taken from Jacques model and entanglement molecular weight was calculated from the topology of the monomer.

In the case of crystallinity prediction the topological approach operates on the level of the previously defined fundamental properties—essentially transforming one kinetic model— $M_n(t)$ —Stage 2 (as defined in Figure 1) to another kinetic model $\chi(t)$ —Stage 2b.

Calculation procedure of the degree of crystallinity is described below with indication of succeeding steps that must be taken. Only the first and last step belong to defined stages, while all the intermediate steps form the transformation procedure:

- Stage 2a: $M_n(t)$
 - Step 1. Molecular weight is obtained from Jacques kinetic model
- Horizontal transformation: topology to M_e
 - Step 2. Backbone rotational degrees of freedom are calculated from the number of single bonds and other structural features of the monomer.⁹

$$N_{BBrot} = N_{BBond} + 0.5N_{FRbond1} + 0.5N_{SFbond2} \quad (21)$$

where N_{BBond} is the number of single bonds in the backbone and not in a ring, $N_{FRbond1}$ is the number of single bonds in the “floppy” ring in the backbone and $N_{SFbond2}$ is the number of single bonds in the “semi-floppy” ring which is not directly bonded to any of the rigid rings

For PA11, we get $N_{BBrot} = 12$

- Step 3. Van der Waals volume V_w (cc/mol) is calculated as function of connectivity indices and correction terms:⁹

$$V_w = 2.28694 X_0 + 17.14057 X_1^V + 1.369231 N_{vdW} \quad (22)$$

$$\begin{aligned} N_{menobar} &+ 0,5N_{mear} + N_{alamid} + N_{OH} + 2N_{cyanide} \\ &- 3N_{carbonate} - 4N_{cyc} - 2,5N_{fused} + 2N_{C=C} + 7N_{Si} \quad (23) \\ &- 8N_{(-S-)} - 4N_{Br} \end{aligned}$$

where $N_{menobar}$ - is the number of methyl groups attached to nonaromatic atoms, N_{mear} is the number of methyl groups directly attached to atoms in aromatic rings, N_{alamid} -is the total number of linkages between amide and similar (e.g., urea) groups and nonaromatic atoms, N_{OH} -is the total number of —OH groups, $N_{cyanide}$ is the number of —C≡N groups, $N_{carbonate}$ - is the number of (—OCOO—) groups, N_{cyc} is the - number of nonaromatic rings with no double bonds along any of the edges of the ring, N_{fused} -is the number of rings in “fused” ring structures, $N_{C=C}$ is the- number of carbon–carbon double bonds excluding those in ring structures. $N_{vdw} = 1$ for PA11 (due to the amide bond present in the monomer) and $V_w = 185.4 \text{ cm}^3/\text{mol}$.

- Step 4. Entanglement molecular weight M_e is calculated from the backbone rotational degrees of freedom, monomer mass, and length and connectivity indices.⁹

$$M_e \approx 1039.7 + 1.36411 * 10^{-23} \frac{N_{BBrot} * M * V_w}{(l_m^3)} \quad [g/mol] \quad (24)$$

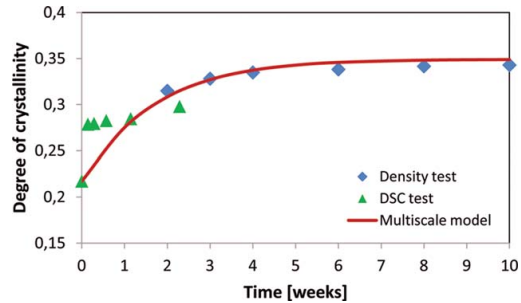


Figure 5. Comparison between modeled and experimental crystallinity evolution. [Color figure can be viewed in the online issue, which is available at wileyonlinelibrary.com.]

where M is the monomer mass (g/mol) and l_m is the monomer length in its fully extended conformation (cm).

The monomer weight of the PA11 is equal 174.2 g/mol. The monomer length l_m can be estimated from trigonometry of the polymer repeat unit or if possible by means of molecular modeling (e.g., Biosym’s Polymer 6.0).⁹ It has been found to be approximately equal to 14 Å for PA11. Finally for PA11 $M_e = 2.27 \text{ kg/mol}$.

The expression for the entanglement molecular weight was obtained by fitting the rubber elasticity theoretical formula to group contribution data.¹²

- Stage 2b: $\chi(t)$

- Step 5. The crystallinity ratio change is calculated as a function of initial crystallinity, molecular weight, and entanglement molecular weight (Fayolle model).⁷

$$\chi(t) = \chi_{c0} + \frac{1 - \chi_{c0}}{\left[\left(\frac{M_{n0}}{M_e} \right)^{\frac{1}{2}} - 1 \right]} \left[\left(\frac{M_{n0}}{M_n(t)} \right)^{\frac{1}{2}} - 1 \right] \quad (25)$$

where χ_{c0} is the- initial crystallinity ratio, M_{n0} is the- initial molecular weight, M_n is the- number average molecular weight.

For our PA11 samples the initial crystallinity ratio was 21.7% and the initial molecular weight was 40.64 kg/mol—obtained from DSC test and viscosity measurements, respectively.⁵

Crystallinity Evolution

The degree of crystallinity was determined with DSC analysis for samples aged up to 2 weeks of exposure. For longer exposure times, crystallinity was calculated from density measurements.⁵

The comparison between modeled and experimental crystallinity evolution is featured in Figure 5. The prediction is fairly accurate for the DSC test and even very accurate for the density based evaluation. It gives an ultimate level of crystallinity:

$$\chi_\infty \approx 35\% \quad (26)$$

if started from initial level of 21.7%. This seems to be a perfect match with the experimental results.

Predicting Density

The density evolution of PA11 during degradation was calculated in five steps, starting with the densities of the amorphous and crystalline phases and crystallinity change $\chi(t)$ as obtained in the previous paragraph. The crystalline phase was assumed impenetrable to water thus with constant properties throughout hydrolytic degradation and its density was obtained experimentally. The density of the amorphous phase was calculated from $T_g(M_n)$ and the topology of the monomer using Seitz formulas for specific volume.¹² The specific volume occupied by the monomer is a structural parameter quantifying molecular packing arrangements.⁹

The steps of the density calculation procedure are described below together with the stages (see Figure 1), they belong to:

- Stage 2: $M_n(t)$ and $\chi(t)$
 - Step 1. The molecular weight is obtained from Jacques kinetic model, and the degree of crystallinity is taken from the multiscale crystallinity model
- Scale bridging: $M_n(t)$ to $V(t)$
 - Step 2. $T_g(M_n)$ is obtained as in Figure 3
 - Step 3. The specific volume $V(T)$ is calculated as a function of temperature, $T_g(M_n)$, connectivity indices and correction terms with one of three procedures, depending on test temperature T and $T_g(M_n)$ of the material:⁹

For : $T \leq T_g(M_n)$, $T_g(M_n) > 298K$:

$$V(T) \approx V(298K) \frac{1.42 T_g(M_n) + 0.15T}{1.42 T_g(M_n) + 44.7} \quad (27)$$

$$V(298K) = 33.58596 X_1^V + 26.518075 N_{Si} \quad (28)$$

where N_{Si} features the number of silicon atoms in the monomer. N_{Si} is an atomic correction term, which are sometimes used to improve accuracy of correlations and has been found to correlate in general case with V (298 K).⁹ However, it is irrelevant for PA11, which does not contain any silicon atoms.

For : $T > T_g(M_n)$, $T_g(M_n) > 298K$:

$$V(T) \approx V(298K) \frac{1.57 T_g(M_n) + 0.3(T - T_g(M_n))}{1.42 T_g(M_n) + 44.7} \quad (29)$$

For : $T > T_g(M_n)$, $T_g(M_n) \leq 298K$:

$$V(T) \approx V(298K) [1 + \alpha_r(298K)(T - 298)] \quad (30)$$

where α_r (298 K) is the coefficient of thermal expansion at room temperature:

$$\alpha_r(298K) \approx \frac{1}{298 + 4.23 T_g(M_n)} \quad (31)$$

For the minor case of $T \leq T_g(M_n)$, $T_g(M_n) \leq 298K$ there are no correlations with proven accuracy.⁹

The expressions for the specific volume were obtained from thermodynamic considerations.⁹ For mechanical properties below the glass transition temperature the

entropy was assumed to be constant, while above the glass transition temperature the material was assumed to behave as a rubber with a mostly entropic mechanical process.¹² Therefore, different expressions for $V(T)$ were obtained for glassy and rubbery polymers. Room temperature $T = 298$ K does not have any specific physical meaning with regard to properties; rather it is merely used as a reference temperature in the model.⁹ The specific volume at a specified temperature was modeled as an extrapolation from the values of $V(T_g)$ and $V(298\text{ K})$.¹² For $T_g(M_n) \leq 298\text{ K}$ the interval between the two temperatures lies in the rubbery region. This forces inclusion of the two different coefficients of thermal expansion to cover the entire spectrum between the room temperature and 0 K. Therefore different expressions must be used in this case to calculate specific volume as well as density and mechanical properties depending on it.⁹

- Stage 3: $\Phi(t)$

- Step 4. The density of the amorphous phase is calculated as a function of monomer weight and specific volume, crystalline density is taken as an input⁵

$$\varphi_a = \frac{M}{V(T)} \quad (32)$$

$$\varphi_c = 1.25 \text{ g/cm}^3, \text{constant}$$

The monomer weight of the PA11 is equal 174.2 g/mol.

- Step 5. Densities of the two phases and crystallinity evolution are combined to obtain density evolution

$$\varphi(t) = \varphi_c * \chi(t) + \varphi_a (1 - \chi(t)) \quad (33)$$

Density Evolution

Figure 6 shows modeled and measured density over the course of degradation. Experimental and modeled values tend to be very similar with a difference of about 1–2% for all aging times. The difference between modeled and experimental trend at shorter times can be explained by the effect of plasticizers. Plasticizers are present in new materials. When the PA11 is placed in water, the plasticizer gets leached out and is replaced by water.⁵ This plasticizer–water interaction is rather complex and it is not accounted for in this model. After about 2 weeks the plasticizer extraction reached a plateau⁵ and the model describes well the density change due to hydrolysis only. From that point onward density change nearly perfectly matches experimental results: the total density changes are controlled by the hydrolysis induced crystallinity increase, since the amorphous phase density hardly differs with aging time. Ideally, the testing should be repeated with non-plasticized material to clearly identify the effect of the plasticizer on the property changes.

DISCUSSION

The model proposed here for the prediction of morphological parameters is not only accurate but also particularly simple to use due to the analytic form of its expressions. Therefore, it can be easily programmed in languages such as MATLAB, calculated

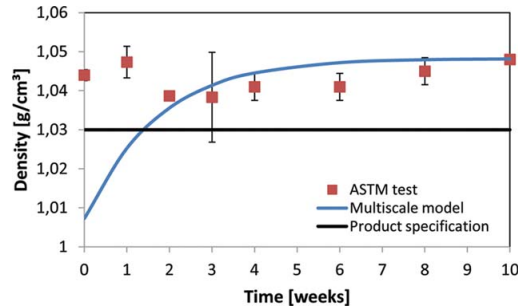


Figure 6. Comparison between modeled and experimental density evolution. [Color figure can be viewed in the online issue, which is available at wileyonlinelibrary.com.]

in Excel spreadsheets or even typed into a handheld calculator.⁹ The predictive power of the model was demonstrated here in the case of PA11 hydrolytic degradation. The model can be applied to any other polymer providing that input parameters for diffusion and structure property models are known and a kinetic model for the specific chemical process in the specific material can be found. The latter somewhat limits the generality of the proposed approach. However, in practice, the kinetic models providing $M_n(t)$ as an output have been developed whenever it was required by industry.²⁴ Consequently such models exist for a wide range of practically important chain-scission processes in different materials.

Input parameters for the morphology evolution predictions can be obtained relatively easy. Data required for structure–property relationship of the amorphous phase (connectivity, mass, and length of the polymer repeat unit) can be directly calculated from the structure of the monomer. The density of the crystalline phase Φ_c and the glass transition temperature T_g are also material constants and can be found in the literature for many polymers.^{9,23} Sample-dependent parameters such as initial molecular weight M_{n0} and initial degree of crystallinity χ_{c0} may also, in the first approach, be taken from the literature for a “typical sample” or ideally be obtained experimentally for the studied specimen. This can be done with viscometric¹⁹ and spectrometric²⁵ measurements for M_{n0} or by XRD,²⁶ DSC,^{5,7} FTIR,⁷ and density^{5,26} tests for χ_{c0} . Among the mentioned parameters initial crystallinity appears to be the most difficult to find in the literature and may be available with good accuracy only for common polymers.

The proposed multiscale model allows obtaining property predictions based on the actual structure of the polymer and is therefore a step forward compared to simple and completely empirical extrapolation of the experimental tests results used today. This model is based on molecular processes although it is still a semiempirical approach, which relies heavily on correlations^{9,12} to obtain properties in the amorphous phase. It is thus unable to provide any insights into actual mechanisms of the property emergence from a certain structure in the microscale. The model can however bring some insights into mechanisms in larger scales as will be discussed in the Part 3 of this study.⁶

Another limitation of the model is its conceptual simplicity. It considers only the most fundamental effects and in the case of morphology predictions provides only the degree of crystallinity ignoring parameters like crystallite size, shape, and orientation. For the calculation of both the density and crystallinity only average molecular mass is used and its distribution is neglected. It should be possible to develop the model further and address these effects in more detail. However, the good agreement with experiments shows that the simple approach taken here is sufficiently accurate for PA11.

The model does not include the effect of depleting plasticizer and therefore could not show this effect as observed during the first 2 weeks of aging for PA11. This is not seen as a severe limitation, because we are mostly interested in long-term predictions. However, when comparing density experimental data with the model, it is important to realize that results may deviate due to the effects of plasticizers. This is not a problem for crystallinity predictions as additive is not expected to have fundamental effect on the cocrystallization process.

Generally the model should be understood as a practical tool aiding engineers with fast and accurate predictions of the morphology. The morphology predictions can be used further to predict global mechanical properties, such as Young's modulus and strength, as will be shown in Part 3 of this paper series.⁶ This extension will provide some insight how the micromechanisms effect macroscopic properties of the semicrystalline polymer.

CONCLUSIONS

A general multiscale methodology for property predictions under aging is presented. Multiscale modeling results for the morphological properties of PA11 are compared with aging tests performed in water at 120 °C. A very good match between model and experiment is obtained for both the density and degree of crystallinity.

The model is easy to use, using simple semiempirical formulas, once the fundamental input parameters are obtained. The fundamental parameters can be found for most common polymers in the literature.

The effect of depletion of plasticizer and low molecular weight components is not modeled and needs to be evaluated separately. This effect is however irrelevant for crystallinity predictions and in the case of PA11 density may only be important in the first 2 weeks of exposure.

The successful prediction of PA11's structural parameters during degradation opens the possibility to predict engineering mechanical properties. An extension of the multiscale model will be presented in the succeeding paper (Part 3). The model provides a faster and less labor extensive engineering alternative to accelerated aging tests.

ACKNOWLEDGMENTS

This work is a part of the “PolyLife” project realized between SINTEF Materials and Chemistry, NTNU, PETROBRAS, ROSEN Group, Kongsberg Oil & Gas Technologies and FMC Technologies.

The authors would like to express their gratitude for the financial support by the Research Council of Norway (grant 193167). Randi Berggren performed accelerated aging and density measurements as part of her master thesis at NTNU.

REFERENCES

1. Teal, J. M.; Howarth, R. W. *Environ. Manag.* **1984**, *8*, 27.
2. Flynn, J. H. *J. Therm. Anal. Calorim.* **1995**, *44*, 499.
3. 4Subsea, PSA no. 0389-26583-U-0032, Revision 5: Unbonded Flexible Ri2sers—Recent Field Experience and Actions for Increased Robustness; 4Subsea AS: Norway, **2013**.
4. Albertsson, A. C.; Barenstedt, C.; Karlsson, S. *J. Appl. Polym. Sci.* **1994**, *51*, 1097.
5. Mazan, T.; Berggren, R.; Jørgensen, J. K.; Echtermeyer, A. T. *J. Appl. Polym. Sci.* **2015**, *132*, 6249.
6. Mazan, T.; Jørgensen, J. K.; Echtermeyer, A. T. *J. Appl. Polym. Sci.* submitted.
7. El-Mazry, C.; Correc, O.; Colin, X. *Polym. Degrad. Stabil.* **2012**, *97*, 1049.
8. Devilliers, C.; Fayolle, B.; Laiarinandrasana, L.; Oberti, S.; Gaudichet-Maurin, E. *Polym. Degrad. Stabil.* **2011**, *96*, 1361.
9. Bicerano, J. Prediction of Polymer Properties; Marcel Dekker AG: New York, **2002**.
10. Flory, P. J. Principles of Polymer Chemistry; Cornell University Press: Ithaca, **1953**.
11. Gordon, M.; Temple, W. B. Chemical Applications of Graph Theory; Academic Press: New York, **1976**.
12. Seitz, J. T. *J. Appl. Polym. Sci.* **1993**, *49*, 1331.
13. van Krevelen, D. W. Properties of Polymers; Elsevier: Amsterdam, **1990**.
14. Fermeglia, M.; Prich, S. *Progr. Org. Coat.* **2007**, *58*, 187.
15. Kremer, K.; Müller-Plathe, F. *Mol. Simul.* **2002**, *28*, 729.
16. Bouvard, J. L.; Ward, D. K.; Hossain, D.; Nouranian, S.; Marin, E. B.; Horstemeyer, M. F. *J. Eng. Mater. Technol.* **2009**, *131*, 041206.
17. Buehler, M. J. Atomistic Modeling of Materials Failure; Springer LLC: New York, **2008**.
18. Halpin, J. C.; Kardos, J. L. *J. Appl. Phys.* **1972**, *43*, 2235.
19. API Technical Report 17TR2, The Ageing of PA-11 in Flexible Pipes; API Publishing Services: Washington, DC, **2003**.
20. Wu, P.; Siesler, H. W. *Chem. Mater.* **2003**, *15*, 2752.
21. Bird, R. B.; Stewart, W. E.; Lightfoot, E. N. Transport Phenomena; Wiley: New York, **1976**.
22. Jacques, B.; Werth, M.; Merdas, I.; Thominette, F.; Verdu, J. *Polymer* **2002**, *43*, 6439.
23. Rilsan® PA11: Created From a Renewable Source; Arkema: France, **2012**.
24. Fayolle, B.; Richaud, E.; Colin, X.; Verdu, J. *J. Mater. Sci.* **2008**, *43*, 6999.
25. Domingos, E.; Pereira, T. M. C.; Filgueiras, P. R.; Bueno, M. I. M. S.; de Castro, E. V. R.; Guimarães, R. C. L.; de Sena, G. L.; Rocha, W. F. C.; Romão, W. *X-Ray Spectrom.* **2013**, *42*, 79.
26. Karacan, I. *Fibers Polym.* **2005**, *6*, 186.

PAPER C

Tobiasz Mazan, Jens Kjær Jørgensen and Andreas Echtermeyer

Aging of Polyamide 11. Part 3: Multiscale model predicting the mechanical properties after hydrolytic degradation

Journal of Applied Polymer Science, Volume 132, Issue 46, pages 13299-13310; Sep 8, 2015

Aging of polyamide 11. Part 3: Multiscale model predicting the mechanical properties after hydrolytic degradation

Tobiasz Mazan,¹ Jens Kjær Jørgensen,² Andreas Echtermeyer¹

¹Department of Engineering Design and Materials, Norwegian University of Science and Technology, Trondheim 7491, Norway

²SINTEF Materials and Chemistry, Oslo 0314, Norway

Correspondence to: T. Mazan (E-mail: tobiasz.mazan@ntnu.no)

ABSTRACT: A holistic general multiscale model of polymer degradation has been applied to predict the mechanical properties of polyamide 11 after the hydrolytic ageing. Results for elastic modulus, tensile strength, and embrittlement threshold have been compared with experimental aging in deoxygenated water at 120°C. For all studied properties the modeled trend is close to the experimental test results confirming hydrolysis induced chain scission and chemicrystallization as the two main mechanisms of property change. This suggests that the multiscale modeling methodology can provide a valuable alternative to accelerated aging tests. The model also indicated that the crystalline phase does play a role in the plastic deformation. Moreover, the mechanical equilibrium between effects of macromolecule degradation and an increased degree of crystallinity has been described. © 2015 Wiley Periodicals, Inc. *J. Appl. Polym. Sci.* **2015**, *132*, 42792.

KEYWORDS: mechanical properties; oil and gas; degradation; polyamides; theory and modeling

Received 30 March 2015; accepted 30 July 2015

DOI: 10.1002/app.42792

INTRODUCTION

Polyamide 11 (PA11) is commonly used as a material for the internal pressure sheaths in offshore flexible risers.¹ It possesses good mechanical and barrier properties; however, it is also known to undergo chemical degradation once exposed to oil field exploration environments, especially water.²

Therefore, long-term performance of the riser under chemical and mechanical factors must be evaluated.³ As of today, long-term performance is evaluated by simple extrapolation of the experimental data for a certain material (here PA11) in the expected environment to lifetimes up to 50 years. No consideration is given to the actual mechanisms behind the degradation process.⁴

Despite extensive laboratory testing; which requires labor, time and resources; actual failure in the field often happens long before (or after) the expected one. Also, without scientific understanding of the processes in the microscale, extrapolation of the results to different application cases is very difficult. In order to improve cost, accuracy, and generality of predictions a general model of degradation is proposed here.

The present article as Part 3 of a series describes the model considering the mechanical properties as a function of previously obtained morphology predictions. This aspect was presented in

Part 2 along with the details of the general modeling methodology proposed.⁵ The experiments were presented in Part 1.⁶

Multiscale Model of Degradation

The multiscale approach is presented here as a way to improve the long-term property evaluations. Many models operating on individual stages of the proposed method exist already. Nevertheless so far the problem has not been treated holistically to form a multiscale model of degradation from the single-scale models. The purpose of this study is to change the state of the art in this research area by linking microscopic degradation induced by chemical factors to macroscale properties of the polymer.

Details of the model both in the general case and as applied to PA11 were presented in the Part 2 of the series.⁵ The following section provides a short summary of this description. The input and output parameters of all constituent models used here for PA11 are also presented later in the article. The multiscale model proposed here consists of four fundamental stages as described below.

Stage 1: Concentration Profile. The concentration profile of the environmental agents (water, oxygen, acids, etc.) in the polymer must be evaluated with time. Normally Fick's diffusion characteristic is assumed; however, if the shape of the

© 2015 Wiley Periodicals, Inc.

concentration profiles is of key importance the validity of this assumption should be checked.

Diffusion in polyamides is usually considered to follow Fick's law.⁷ The diffusion coefficient of water in Polyamide 11 was taken from the literature.⁷ Its value shows, that for PA11 aged in water diffusion proceeds very fast.^{1,7} Therefore the environmental agent is uniformly distributed within the material. Polyamide 11 will be here considered to be completely saturated, thus Stage 1 will not be considered in the later parts of the article. It is assumed that the amorphous part will absorb water while the crystalline part remains mostly unaffected.

Stage 2: Kinetic Model—Molecular Level. The effect of chemical action of the environmental agent on the polymer molecular properties with time must be found. This is a key part of the methodology as it predicts the molecular response in the long-term perspective for which direct empirical evaluation would be impractical or impossible. The most important property changes addressed in this task are the molecular weight decrease of the amorphous phase and the degree of crystallinity increase.^{5,6}

Jacques kinetic model was chosen to calculate the kinetics of hydrolytic chain-scission due to its confirmed accuracy and relative simplicity.⁸ Chain scissions result in decreased molecular weight, which in turn decreases stiffness in the amorphous phase and will eventually cause the embrittlement of the entire material.⁹

The molecular weight evolution in Jacques kinetic model is governed by the following equation:⁸

$$M_n(t) = M_{ne} \frac{M_{n0}^{-1} + M_{ne}^{-1} + (M_{ne}^{-1} - M_{n0}^{-1}) \exp(-Kt)}{M_{n0}^{-1} + M_{ne}^{-1} - (M_{ne}^{-1} - M_{n0}^{-1}) \exp(-Kt)} \quad (1)$$

where M_{ne} —equilibrium molecular mass; M_{n0} —initial molecular mass; K —experimental pseudo rate constant.

The Jacques kinetic model was presented in more detail in a previous article⁵ of the series as well as in the original reference.⁸

Moreover the chain scissions tend to destroy the entanglement network in the amorphous phase and liberate small molecular segments, which diffuse towards the crystals surface and initiate chemicrystallisation.¹⁰ The Fayolle model predicts the degree of crystallinity as a function of aging time. Required input includes the initial crystallinity χ_{c0} , molecular weight evolution $M_n(t)$, and entanglement molecular weight M_e :¹⁰

$$\chi(t) = \chi_{c0} + \left[\frac{1 - \chi_{c0}}{\left(\left(\frac{M_{n0}}{M_e} \right)^{\frac{1}{2}} - 1 \right)} \right] \left[\left(\frac{M_{n0}}{M_n(t)} \right)^{\frac{1}{2}} - 1 \right] \quad (2)$$

Stage 2 to Stage 3: Scale Bridging. Individual models are designed to function in a specific scale range. In order to couple single-scale models and develop larger multiscale model a scale bridging procedure is required. In the case of the degradation model proposed here only one such procedure is needed. The dependence of the glass transition temperature on molecular weight $T_g(M_n)$ must be found to integrate the kinetic model

with the structure–property relationship. $T_g(M_n)$ can be obtained with the Fox and Flory equation:^{9,11}

$$T_g(M_n) \approx T_g^\infty - 0.002715 \frac{(T_g^\infty)^3}{M_n} \quad (3)$$

where T_g^∞ is the hypothetical T_g for infinite molecular mass. T_g^∞ is a material parameter that can be calculated substituting the initial T_g and M_n into the former equation.

Stage 3: Structure–Property Relationship. The microstructure–property relationship yielding local mechanical properties of the polymer must be found. The multiscale approach proposed here used topological formalism utilizing connectivity indices defined via graph theoretical concepts as primary descriptors of the polymer repeat units. Topology can be seen as a pattern of interconnections between atoms in a polymer repeat unit. Connectivity indices give information on the electronic configuration and the coordination number for all atoms in the monomer.⁹

In order to quantitatively predict polymer properties from the microstructural data connectivity parameters are correlated with the experimental results of so called fundamental properties.⁹ Fundamental material properties are properties in the microscale such as volume occupied by the molecule, cohesive energy, etc. They are further combined into derived properties on the macroscale such as density or elastic constants.⁹ Formulas for derived properties are obtained by fitting the experimental data with equations from thermodynamic and molecular theories.

It is argued that this method is more practically feasible than alternative approaches, e.g., molecular dynamics simulations or group contribution technique. Molecular dynamics must deal with time limitation and scale bridging issues.^{12–14} Group contribution technique cannot be used if estimating the value of even a single group contribution is problematic. This serious limitation actually triggered the development of the topological approach.^{9,15}

The structure of the PA11 repeat unit was analyzed to obtain the topology data.⁹ The following values of the connectivity indices were found and will be used in the model:⁹

$$X_0 = 9.3555, \quad X_0^V = 8.4793 \quad (4)-(7) \\ X_1 = 6.3938, \quad X_1^V = 5.6612$$

Generally X_0 and X_1 provide information on coordination numbers while X_0^V and X_1^V quantify details of the electronic configuration in the monomer.

The exact procedures required to get the structure–property relationships in the Stage 3 are different for each property to be obtained. They are described in detail for the mechanical properties in the later parts of this article. The model for morphology predictions was already featured in the previous article.⁵

Stage 4: Global Properties. In the final stage the local properties must be combined into global engineering parameters. This can be done with several methods such as micromechanical finite element analysis or composites theory, e.g. Halpin and Kardos.¹⁶

Table I. Constituent Models of Multiscale Approach for Prediction of Various Properties

Property modeled (multiscale approach)	Constituent models
Modulus	Jacques ² Fox and Flory ^{2,3} Bicerano ^{2,3} topological Seitz ³ Rubber ³ elasticity Crystallinity multiscale ³ Halpin-Tsai ³ Water softening ³
Tensile strength	Jacques ² Fox and Flory ^{2,3} Bicerano ^{2,3} topological Wu ³ Seitz ³ Halpin-Tsai ³
Embrittlement	Jacques ² Fox and Flory ^{2,3} Bicerano ^{2,3} topological Seitz ³ Tensile strength multiscale ^{2,3} Kausch ²⁻⁴
Mechanical equilibrium ^a	Modulus ³ amorphous multiscale Crystallinity ³ multiscale Halpin-Tsai ^{2,3}

^aMolecular weight as an independent variable; numbers indicate stage or scale bridging in which certain model was introduced—reference in the main text.

In the case of PA11 aging described here there is an even distribution of water through the body as the diffusion happens very quickly. Besides this the current modeling approach has seen the amorphous matrix as perfectly homogenous with evenly distributed crystallites. Therefore properties will be uniform throughout the material and global engineering properties do not need to be evaluated. Because of this Stage 4 will not be considered at any point later in the article.

PREDICTION OF THE PA11 MECHANICAL PROPERTIES

This section contains detailed property prediction procedures for the Young's modulus, yield strength, brittleness, and mechanical equilibrium. It also features comparison between model and experiment. An analogous section in Part 2 of this article series considered the density and crystallinity evolution.⁵

Experimental results relevant for the modeling described here were reported in detail in previous work.⁶ They are reported with error bars representing one standard deviation of parallel laboratory test results. It is supposed to give a statistically meaningful comparison between model predictions and laboratory testing.

Input and Output Parameters

Table I lists the constituents of multiscale models applied in this article to calculate mechanical properties of PA11. Table II features input parameters for these constituent models, their values to be used with the property predictions along with reference and the output parameters produced by the model.

Input parameters can be generally divided into constants and variables. The constants are the parameters specific for a certain polymer system. The variables describe conditions specified by the application. Such variables include aging conditions (hydrolysis temperature and time), initial parameters of the studied sample (initial molecular weight and degree of crystallinity), and finally test temperature in the case of tensile mechanical properties.

Predicting Elastic Modulus

The decrease in amorphous Young's modulus due to chemical action can be estimated by taking into account the rate of chain scission from stage two of the present methodology and by relating it to the number average molecular weight. Then the change in the glass transition temperature can be found and used to express Poisson's ratio and finally elastic constants of the polymer.^{20,21}

The procedures to calculate the polymer's elastic modulus of the amorphous phase in three different temperature regimes (glassy, rubbery, and leathery state) have been established.⁹ Subsequently the obtained amorphous modulus, the assumed crystalline modulus and the previously calculated crystallinity evolution $\chi(t)$ have been combined with the Halpin-Tsai short fiber composite model.¹⁶ The crystalline phase is considered impenetrable to water,¹ therefore it is expected to have constant morphology and properties during degradation. Moreover the present study followed the approximation used in El-Mazry's work.¹⁰ It was assumed that the secondary lamellae created in the process of cemicrystallization possess the physical and thermal characteristics of the initial primary lamellae.

The modulus calculation procedure is described below showing the steps that must be taken and stages they belong to:

Input from Microscale Models.

- Step 1. First the specific volume must be obtained as described in "Predicting Density" chapter of the previous article⁵ (Part 2). Conditions corresponding to different polymer states are as follows:

- Glassy state for:

$$T \leq T_g, T_g > 298 \text{ K}$$

- Rubbery state for:

$$T > T_g, T_g > 298 \text{ K}$$

or

$$T > T_g, T_g \leq 298 \text{ K}$$

- Step 2. Entanglement molecular weight M_e and $\chi(t)$ are calculated as described in "Predicting Crystallinity" section of the previous article⁵ (Part 2).

Table II. Input Parameters, Their Values, and Output of Constituent Models in Multiscale Approach

Model	Input parameters	Values chosen	Output parameters
Jacques	T_{hyd} —hydrolysis temperature M_{n0} —initial molecular weight t —hydrolysis time T_g^M —initial T_g for specified molecular weight $M_n(t)$	120°C—slightly above riser working conditions ² 40.64 kg/mol—experiment ⁶ (part 1) Independent variable 45°C for 40.64 kg/mol—literature ² T_g for M_{n0} Jacques model	$M_n(t)$ —number average molecular weight $T_g(M_n)$ —glass transition temperature
Fox and Flory			
Bicerano topological	$T_g(M_n)$	Fox and Flory model	E_{coh} , V_w , V , M_e , φ_a —see input parameters below
	Connectivity	$X_0 = 9.3555$, $X_0^V = 8.4793$, $X_1 = 6.3938$, $X_1^V = 5.6612$ from literature ⁹	
	M —monomer mass	174.2 g/mol from literature ⁹	
	l_m —monomer length	14.05 Å—self-calculated from geometry of monomer	
	T —test temperature	25°C—Room temperature assumed	
	$T_g(M_n)$	Fox and Flory model	$B(T)$, $E(T)$, $G(T)$ —bulk, Young's and shear moduli for glassy state $\sigma_f(T)$ —brittle fracture stress
Seitz	E_{coh} —cohesion energy V_w —Van der Waals volume V —specific volume at test temperature	84.7 kJ/mol—Bicerano model 119.8 cm ³ /mol—Bicerano model 185.4 cm ³ /mol—Bicerano model	
Rubber elasticity	M_e —entanglement molecular weight + Same as Seitz model	2.27 kg/mol—Bicerano model	$B(T)$, $E(T)$, $G(T)$ —bulk, Young's and shear moduli for rubbery state
Fayolle	X_{co} —initial crystallinity ratio M_{n0} , $M_n(t)$ M_e	21.7%—experiment ⁶ (part 1) Jacques model Bicerano model	$X_c(t)$ —degree of crystallinity E_{sc} —modulus of the semicrystalline polymer
Halpin-Tsai	E_a —amorphous phase modulus E_c —crystalline phase modulus $X_c(t)$ A_f —crystalline phase aspect ratio $T_g(M_n)$	Seitz model 25 GPa ^a —literature ¹⁷ Fayolle model 1—ideal spherulites assumption Fox and Flory model Bicerano model	σ_a —amorphous tensile strength
Wu	E_{coh} , V C_∞ —characteristic ratio		

Model	Input parameters	Values chosen	Output parameters
Water softening	E_{sc}	Halpin-Tsai model k_{sat} —water softening factor (saturated state) k_{bnd} —softening factor of "bound water" ^d k_{res} —softening factor of the residual plasticizer ^e	E_{sat} —modulus corrected for water or plasticizer content 0.78—obtained from E (wt %) relation ^c , literature ¹⁹ 0.93—obtained from E (wt %) relation ^c , literature ¹⁹ 0.82—obtained from reported $E_{plast} - E_{unplast}$, literature ²
Kausch	M_e		MW_e^{brittle} —embrittlement threshold

^a α form of PA6—expected similar to PA11.^b For PA66.^c Softening effect of certain water content is assumed the same for all polyamides (difference arises solely from variation in saturation rates and levels).^d As in Langmuir desorption model¹⁹ (0.5% assumed).^e 2% assumed, experiment^f (part 1).^f Softening effect of plasticizer is assumed linear with respect to its content, literature.¹⁹

Stage 3: E(t) Amorphous. Glassy state. The bulk modulus and Poisson's ratio formulas for a glassy state polymer operate in the temperature range of:⁹

$$T \leq T_g - 20 \text{ K}, \quad T_g > 298 \text{ K}$$

For the minor case of $T \leq T_g - 20 \text{ K}$, $T_g \leq 298 \text{ K}$ there are no correlations with proven accuracy.⁹

- Step 3. The bulk modulus is calculated as a function of specific volume and topology of a monomer:⁹

$$B(T) \approx 8.23333 E_{coh1} \left[\frac{5V(0K)^4}{V(T)^5} - \frac{3V(0K)^2}{V(T)^3} \right] \quad (8)$$

where E_{coh1} is the Fedor's type cohesive energy (J/mol).

The cohesive energy can be expressed with the following formula:

$$E_{coh1} = 9882.5 X_1 + 358.7 (6 N_{\text{atomic}} + 5 N_{\text{group}}) \quad (9)$$

N_{atomic} and N_{group} are the correction terms that can be calculated as follows:

$$N_{\text{atomic}} = 4N_{(-S-)} + 12N_{\text{sulfone}} - N_F + 3N_{\text{Cl}} + 5N_{\text{Br}} + 7N_{\text{cyanide}} \quad (10)$$

where: $N_{(-S-)}$ —number of sulfur atoms in the lowest oxidation state, N_{sulfone} —number of sulfur atoms in the highest oxidation state, N_F , N_{Cl} , and N_{Br} —total numbers of fluorine, chlorine, and bromine atoms, N_{cyanide} —number of nitrogen atoms with $\delta=1$ and $\delta^V=5$.

$$\begin{aligned} N_{\text{group}} = & 12N_{\text{hydroxyl}} + 12N_{\text{amide}} \\ & + 2N_{[\text{non-amide-(NH-unit)}]} - N_{(\text{alkyl ether-O-})} - N_{\text{C=C}} \\ & + 4N_{[\text{non-amide-(C=O)- next to nitrogen}]} \\ & + 7N_{[\text{-(C=O)- in carboxylic acid, ketone or aldehyde}]} + 2N_{[\text{other-(C=O)-}]} \quad (11) \\ & + 4N_{[\text{nitrogen atoms in six membered aromatic rings}]} \end{aligned}$$

where N_{hydroxyl} denotes the total number of $-OH$ groups in alcohol or phenol environments and N_{amide} is a total number of amide groups.

For PA11 $N_{\text{group}}=12$ and $E_{coh1}=84.7 \frac{\text{kJ}}{\text{mol}}$. Several atom types have been found to correlate in the general case with E_{coh1} , but it is irrelevant for PA11 since $N_{\text{atomic}}=0$.

The expression for the bulk modulus was obtained from molecular and thermodynamic considerations.²⁰ Polymer repeat units were assumed to be surrounded by a mean field as described by the Lennard-Jones potential function:²²

$$V(r) = 4\varepsilon \left[\left(\frac{\sigma}{r} \right)^{12} - \left(\frac{\sigma}{r} \right)^6 \right] \quad (12)$$

where $V(r)$ is the intermolecular potential between the two molecules, ε is the potential well depth, σ is the van der Waals

Table II. Continued

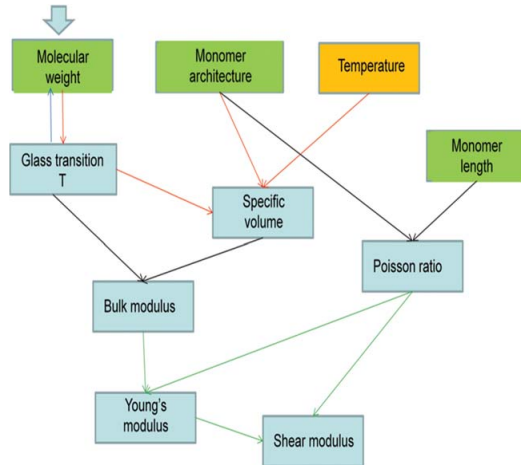


Figure 1. Flow chart for the modulus calculation. Green boxes are related to the architecture of the molecule and blue boxes describe the macro properties of the polymer. [Color figure can be viewed in the online issue, which is available at wileyonlinelibrary.com.]

radius, and r is the distance of separation between both particles.

Based on this the total potential energy of a system was defined and its partial derivative with respect to the specific volume was obtained. The latter was then substituted into the thermodynamic equation state for pressure P below the glass transition temperature. Finally by taking the derivative of the pressure and multiplying the result by the specific volume (since $B = -V[(dP)/(dV)]_T$)²⁰ an expression for the bulk modulus as a function of fundamental properties is obtained.

- Step 4. The Poisson's ratio $\nu(T)$ is calculated as a function of T_g , temperature, connectivity indices and monomer length:⁹

$$\nu(T) \approx \nu_0 + \frac{50T}{T_g} \{0.00163 + \exp[0.459(T - T_g - 13)]\} \quad (13)$$

$$\nu_0 = \nu(298 \text{ K}) - \frac{14,900}{T_g} \{0.00163 + \exp[0.459(285 - T_g)]\} \quad (14)$$

$$\nu(298 \text{ K}) = 0.513 - 3.054 \times 10^{-6} \sqrt{\frac{V_w}{l_m}} \quad (15)$$

where V_w is the van der Waals volume (mL/mol) and l_m is a monomer length in its fully extended conformation (cm).

$\nu(T)$ was obtained as a fitting function between the experimental Poisson's ratio and temperature, ν_0 is merely used to simplify the notation.²⁰ $\nu(298 \text{ K})$ was obtained as a fit between the experimental Poisson's ratio at room temperature and the cross-sectional area of the polymer repeat unit.²⁰

- Step 5. Young's and shear moduli are expressed in relation to the bulk modulus and Poisson's ratio

Finally the Young's modulus is found from elasticity theory for isotropic materials:

$$E = 2(1 + \nu)G = 3(1 - 2\nu)B \quad (16)$$

Properties here are assumed isotropic at the local level.

Figure 1 summarizes the calculation of the elastic moduli in a form of a flow chart. It shows that from the architecture of the macromolecule (green), the temperature (orange) and the initial T_g it is possible to calculate a wide range of polymer properties (blue).

Rubber state. The rubbery state formulas mentioned in this paragraph function in the temperature range $T \geq T_g + 30 \text{ K}$ for the shear and bulk modulus and $T \geq T_g$ for Poisson's ratio. They are obtained from rubber elasticity theory as discussed in Ref. 9.

- Step 3. The shear modulus is calculated as a function of temperature, density, specific volume, and M_e :

$$G_N^0(T) = \frac{\rho(T) \times RT}{M_e} \text{ (MPa)} \quad (17)$$

$$\rho(T) = \frac{M}{V(T)} \text{ (g/mL)} \quad (18)$$

The modulus is here defined only for temperatures in the rubbery plateau regime, inception of which is assumed to be at $(T_g + 30 \text{ K})$. This expression does not apply to temperatures in the terminal zone, where a steep decrease of modulus occurs.⁹ Since the onset of the terminal zone is not clearly defined, a practical approach often involves calculating the modulus for the inception point ($T_g + 30 \text{ K}$) and assuming the obtained value for an arbitrary rubbery plateau.⁹

- Step 4. The bulk modulus is calculated from the specific volume and connectivity indices

$$B(T) = \frac{\frac{205V(T)}{V_w}}{\left[\frac{V(T)}{V_w} - 1.27\right]^2} - 2329 \left[\frac{V_w}{V(T)}\right]^2 \quad (19)$$

where V_w is the van der Waals volume.

The expression for the bulk modulus in the rubbery state was obtained in an analogous way to the glassy state. The thermodynamic equation of state for pressure P above the glass transition temperature was used.

- Step 5. The Poisson's ratio is obtained from the bulk and shear moduli

$$\nu = \frac{3B(T) - 2G(T)}{6B(T) + 2G(T)} \quad (20)$$

- Step 6. The Young's modulus is obtained from the shear modulus and Poisson's ratio

$$E(T) = 2[1 + \nu(T)] \times G_N^0(T) \quad (21)$$

Leathery state. Between the glassy and rubbery domain the transition “leathery” period can be identified. This is modeled as a linear interpolation between the left boundary considered glassy and a right one assumed rubbery:

$$\text{For: } T_g - 20 \text{ K} < T < T_g + 30 \text{ K}$$

$$E(T) = E_{T_g-20\text{K}} - \frac{E_{T_g-20\text{K}} - E_{T_g+30\text{K}}}{50\text{K}} (T - T_g + 20 \text{ K}) \quad (22)$$

Stage 3: E(t) Semicrystalline. Halpin-Tsai model.

- Step 1. The Young's modulus of the amorphous phase is taken from the topological approach for either the glassy, the rubbery, or the leathery state. The crystalline modulus is taken from the literature.¹⁷ It is assumed not to change due to the exposure to water, because water does not penetrate the crystalline region.

$$E_a(t) \leftarrow \text{Elastic modulus model (glassy, rubbery, or leathery)} \\ E_c = 25 \text{ GPa, constant} \quad (23)$$

- Step 2. The Halpin-Tsai short fiber composite model combines moduli of the two phases and the crystallinity change χ (t) into a global modulus of the material:¹⁶

$$E_l(t) = E_a(t) \frac{1 + (2A_f)\eta_l\chi(t)}{1 - \eta_l\chi(t)} \quad (24)$$

$$\eta_l = \frac{(E_c/E_a) - 1}{(E_c/E_a) + 2A_f} \quad (25)$$

$$A_f = l_f/d_f \quad (26)$$

where E_l —longitudinal modulus of the material, A_f —aspect ratio of the crystallite, l_f —average length of the crystallite, d_f —average diameter of the crystallite.

Because crystallites are assumed to be perfect spherulites $A_f = 1$ in this approach: $E_l = E_t = E_{\text{random}}$.

Softening effect of water saturation. Water is known to act in a similar way as a plasticizer, thus its absorption shall have a softening effect.¹⁹ An empirical relationship with regard to the softening can be written in the form of:

$$E_{\text{sat}}(t) = k(t) \times E_0 \quad (27)$$

where $E_{\text{sat}}(t)$ —Young's modulus of water saturated semicrystalline polymer, E_0 —initial Young's modulus of semicrystalline polymer, $k(t)$ —time dependent softening factor obtained from experimental study of isothermal water absorption.¹⁹

The above can be also used for other plasticizers as long as experiments necessary to obtain $k(t)$ have been performed. A summary of relevant softening factors is given in Table II.

The multiscale model used here estimates the effect of plasticizer for PA11. It incorporates experimental results reporting as much as 29% of remaining plasticizer after exposure in 120°C and a relative difference in the modulus between plasticized and unplasticized PA11 as given in the Rilsan documentation.²⁶ The assumption of the linear softening with respect to plasticizer content is based on water induced softening, which was found to be nearly linear before reaching a modulus plateau region.¹⁹

Elastic Modulus Evolution

The Young's modulus obtained from the modeling has been compared with an experimental stress strain curve measured at a displacement rate of 2 mm/min. The secant modulus was calculated as the slope between 0.2% and 0.5% strain according to common practice in polymer science. The modulus was also obtained as the storage modulus tested at 2 Hz in a Dynamic Mechanical Thermal Analysis (DMTA). Samples used were aged more than 7 days to assure effects of plasticizer become largely reduced and they were subsequently dried. Figure 2 summarizes the comparison between the multiscale model and experiment (tensile test, DMTA) for the Young's modulus.

The predicted modulus is in good agreement with the experimental results from the DMTA test, but it is significantly overestimated compared with the tensile test. Since the tensile test is done at a much lower strain rate than the DMTA testing a change in modulus is to be expected for a viscoelastic polymer.

The multiscale model calculates the theoretical Young's modulus; however, it does not distinguish between different deformation modes and it does not account for loading rate dependent properties. Within the model presented here tensile, flexural and storage moduli should all yield the same value. The parameters used in this model were typically obtained for testing rates of the DMTA. The T_g reported here for PA11 is a key parameter obtained by DMTA. T_g is loading rate dependent and this aspect has not been modeled. It is, therefore, reasonable that the dynamic storage modulus better accounts for the viscoelastic nature of polymers than the modulus obtained from the standard tensile test.

The experimental data (taken with uncertainty values) can be interpreted as monotonically increasing with an eventual plateau and this characteristic is well predicted with the model. Therefore, chemicrystallization and chain scission are confirmed as the two governing mechanisms of stiffness evolution (following additive extraction). Some discrepancy between the model and DMTA result occurs only for the first week of aging, since at this time a significant amount of plasticizer is still in the sample. A possible sharp stiffness increase between 4 and 6 weeks of aging (as observed for the tensile modulus) has been ruled out after subsequent DMTA tests.

If only the tensile data is available the model can be directly used to estimate the time to reach the modulus plateau during hydrolysis. As a practical approach it could also be possible to measure the tensile modulus experimentally, which can be easily done. The change of the modulus with time can then be predicted with the theory described here. Including viscoelastic effects and using time temperature superposition is planned for the future.

Predicting Tensile Yield Strength

The multiscale model predicting yield strength incorporates the Wu equation for the amorphous phase coupled with a computational procedure (converting tensile strength into modulus via an empirical relation, calculating global modulus with Halpin-Tsai equations and finally converting it back to strength) for a

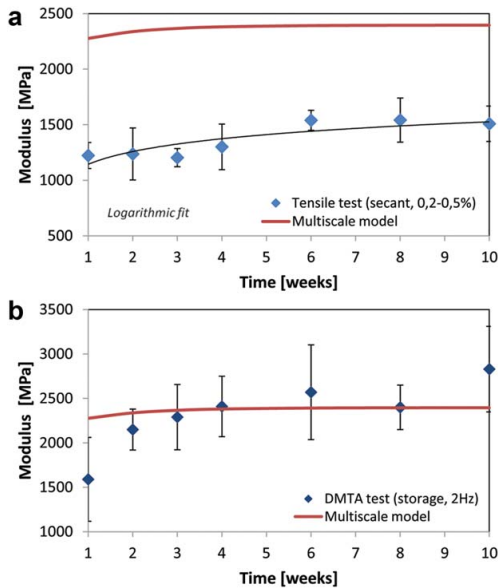


Figure 2. Comparison between modeled and experimental Young's modulus of the water saturated samples in (a) static tensile and (b) dynamic mechanical deformation. [Color figure can be viewed in the online issue, which is available at wileyonlinelibrary.com.]

semicrystalline polymer. The effect of water and residual plasticizer was neglected.

This method considers glassy polymers at temperatures of at least 20°C below their glass transition temperatures.

The tensile yield strength calculation procedure is described below:

- Step 1. T_g , E_{coh1} , and $V(T)$ are calculated as described in the previous sections. The characteristic ratio of polymer macromolecule C_∞ and crystalline modulus E_c are obtained from the literature.^{17,18}

Stage 3: $\sigma_a(t)$.

- Step 2. The amorphous tensile yield strength is calculated from the Wu model:⁹

$$\sigma_a(t) = 10^{(-3.36 + C_\infty)} \left(\frac{E_{coh1}}{V(T)} \right) \quad (28)$$

The yield stress σ_a has been shown to be proportional to $\Delta T = T_g - T$ and $\frac{E_{coh1}}{V(T)}$, where T is the testing temperature and $\frac{E_{coh1}}{V(T)}$ the cohesive energy density.²³ This proportionality is due to interchain effects on the yield stress. At the yield point of tensile deformation some bonds start to rotate from *cis* to *trans* conformation causing irreversible extension of some chains segments. Therefore experimental values of the yield stress were plotted against intrinsic chain flexibility quantified by the characteristic ratio C_∞ in order to obtain the final formula.²³

Stage 3: $\sigma_{sc}(t)$.

- Step 3. The tensile yield stress of the amorphous phase is converted to Young's modulus via an empirical relationship,⁹ the crystalline modulus is again taken from the literature¹⁷

$$E'_a = \frac{\sigma_a(t)}{0.028} \quad (29)$$

$$E_c = 25 \text{ GPa, constant}$$

- Step 4. The Halpin-Tsai short fiber composite model is combining moduli of the two phases into a global modulus of the material:¹⁶

$$E_l(t) = E'_a \frac{1 + (2A_f)\eta_l\chi(t)}{1 - \eta_l\chi(t)} \quad (30)$$

where E'_a is a amorphous tensile strength converted to modulus.

- Step 5. The modulus is converted back to strength obtaining an estimate for the semicrystalline polymer:

$$\sigma_{sc}(t) = E_l(t) \times 0.028 \quad (31)$$

Tensile Strength Evolution

The experimental tensile strength was obtained by dividing the maximum load in each stress-strain curve by the original cross-sectional areas. Figure 3 summarizes the tensile strength comparison between the multiscale model and tensile test results. Predicting tensile strength turns out to be less problematic than it is the case for the tensile elastic modulus. Here the exact strength values as well as their change with time are modeled fairly well.

The multiscale model incorporating the crystalline phase predicts the experiments much more closely in both absolute value and trend than one for the amorphous phase only. This suggests that the crystalline phase does play an important role in the plastic deformation as opposed to the view that this is solely a matter of the amorphous phase. The above hypothesis could be experimentally tested in the future by qualitatively comparing the shape of crystallites in undeformed and deformed samples.

Predicting Embrittlement

Polymeric materials often undergo embrittlement during chemical degradation. Two semiempirical methods estimating the M_n at which the aged material becomes brittle are proposed here. The models give rough estimates of embrittlement conditions.

Yielding and Brittle Fracture Balance. The yielding-brittle fracture balance method uses local properties of the material (stage 3) to obtain the molecular parameter (stage 2) tied with macroscopic behavior of embrittlement. The embrittlement threshold calculation procedure employing this method is described below:

- Step 1. The specific volume is calculated as described in previous sections.
- Step 2. Brittle fracture of the semicrystalline polymer is calculated as a function of specific volume and monomer length:⁹

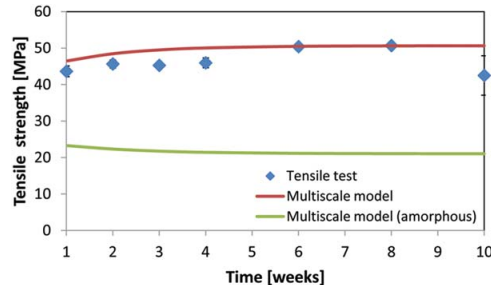


Figure 3. Comparison between modeled and experimental tensile strength evolution. [Color figure can be viewed in the online issue, which is available at wileyonlinelibrary.com.]

$$\sigma_f(T) \approx \frac{2.288424 \times 10^{11} \times l_m}{V(T)} \quad (32)$$

The brittle stress to failure is given by the number of bonds times the strength of an individual bond minus the effect of structural defects concentrating high stress in local areas.²⁰ Therefore, plotting the number of backbone bonds per unit area against the measured brittle strength and a subsequent regression analysis yield the theoretical strength of a fully extended (M_w^∞) linear polymer. Subsequently, the $\frac{M_w}{M_e}$ ratio at which the strength goes to zero was used to obtain the molecular weight dependent brittle fracture stress from the theoretical stress.²⁰

- Step 3. The yield stress of the semicrystalline polymer is calculated with the procedure involving the Wu equation:

$$\sigma_y(T) \leftarrow \text{tensile strength model}$$

- Step 4. A lower value stress is assigned as a governing mechanism

$$\sigma_f(T) > \sigma_y(T) \text{ or } \sigma_f(T) < \sigma_y(T)$$

- Step 5. The embrittlement threshold is estimated.

Embrittlement happens, when the time of exposure causes a reduction of molecular weight ($MW_{y-f}^{\text{brittle}}$) for which the criterion $\sigma_f(T) < \sigma_y(T)$ is reached.

This method takes crystallinity into account by using yield strength values (dependent on crystallinity ratio).

Cohesion Based Evaluation. Macromolecules inside the polymer can move apart easily, when cohesion is low. This means they eventually get completely separated. When the same force is exerted to material with high cohesion, the molecules would still stick together. In polymers the entanglement network creates an important part of intermolecular cohesion forces, determining the plastic deformation responsible for ultimate elongation.¹⁰ When the number of entanglements per macromolecule decreases due to degradation, the Van der Waals interactions remain as the main intermolecular forces. The Van der Waals forces alone are not strong enough for allowing plastic deformation. This stage marks the onset of a brittle material.

An appropriate criterion has been developed by Kausch:²⁴

$$MW_e^{\text{brittle}} \approx 5 M_e \quad (33)$$

The entanglement molecular weight has been estimated with the topological model. This method converts the microstructural parameter (stage 2) to a molecular parameter tied to macroscopic behavior of brittleness.

In the cohesion based evaluation crystallinity is neglected as influencing brittle fracture. The embrittlement is considered to happen because of weak intermolecular forces in the amorphous phase. Consequently, once the amorphous phase gets brittle there is nothing to hold the crystalline parts together anymore.

Embrittlement Threshold Evaluation

The first of the embrittlement predicting methods proposed here calculates the molecular weight for which yielding and fracture stresses are equal marking the onset of PA11's brittle failure domain:

$$MW_{y-f}^{\text{brittle}} \approx 9.2 \text{ kg/mol} \quad (34)$$

The second method calculates molecular weight for which PA11 entanglement network is no longer able to allow plastic deformation:

$$MW_e^{\text{brittle}} \approx 11.4 \text{ kg/mol} \quad (35)$$

These modeled values can be compared with the experimentally established Corrected Inherent Viscosity (CIV) based failure criterion of 1.05 dL/g as given in the American Petroleum Institute (API) standard.¹ The viscosity value can be converted to molecular weight with Jacques equation:⁸

$$MW_{\text{API}}^{\text{brittle}} \approx 13.8 \text{ kg/mol} \quad (36)$$

$MW_{\text{API}}^{\text{brittle}}$ is an industrial, experience based criterion giving a molecular weight below which PA11 exhibits brittle behavior. The modeled embrittlement thresholds mark the minimum molecular weight for which any plastic deformation is theoretically possible. The plateau for PA11 hydrolysis is about 17 kg/mol¹⁶—corresponding to initial service acceptance criterion of 1.2 dL/g given by API.^{1,8} This means that brittle fracture usually involves additional mechanisms of chain scission.

The two models described above are semiempirical and more work is needed to determine which approach is best. Also, the experimental embrittlement definition used in the API standard is not ideal. However, the advantage of the theoretical methods given above is their ability to estimate a rough preliminary brittle failure criterion of various polymers without the need for extensive testing as in the conventional CIV-mechanical method described by API.

Predicting Mechanical Equilibrium

Following plasticizer depletion the stiffness evolution is modeled as a competition between degradation of the amorphous phase and an increasing crystallinity ratio. Initially mechanical properties are controlled by chemocrystallization, however, the chain scission gradually takes control over time.

Mechanical equilibrium is here defined as the molecular weight $MW_{\text{mech}}^{\text{eq}}$ corresponding to a point on a stiffness versus time curve,

where effects of degradation and chemicrystallization on the modulus cancel each other out. This is also the molecular weight for which the maximum modulus point during aging occurs. After crossing that point of time degradation takes control. Mechanical equilibrium has been found by observing how the modeled elastic modulus changes with decreasing molecular weight directly rather than indirectly via time and the kinetic model.

Mechanical Equilibrium Evaluation

Equilibrium of degradation and chemicrystallization effects on PA11 stiffness is predicted here as:

$$\text{MW}_{\text{mech}}^{\text{eq}} \approx 10.8 \text{ kg/mol} \quad (37)$$

This is molecular mass for which the highest value of modulus is obtained during aging. A further decrease of molecular weight would see chain scission taking control over stiffness changes. This does not happen for the studied samples, since the hydrolysis plateau is around 17 kg/mol.⁶ However, it may happen if additional degradation mechanisms are involved, such as oxidation or UV exposure.

DISCUSSION

In general the model presented here is best understood as a practical tool providing engineers with fast and accurate predictions of mechanical properties. The model is not only accurate, but also particularly easy to use due to the analytic form of its formulas. The fundamental input parameters are available for most common polymers in the literature. The proposed approach can be applied to every polymer as long as a kinetic model for the specific chemical process in the specific material is known. Such models exist for a wide range of practically important degradation processes in various materials.

Input parameters for the mechanical properties predictions can be obtained relatively easy. Information needed for the structure–property relationship of the amorphous phase (connectivity, mass and length of the polymer repeat unit) can be directly obtained from the architecture of the polymer's repeat unit. Parameters such as initial molecular weight M_{n0} and initial degree of crystallinity χ_{c0} depend on the studied specimen. M_{n0} can be evaluated with viscometric¹ and spectrometric²⁵ measurements while by χ_{c0} may be obtained with XRD,²⁶ DSC,^{6,10} FT-IR,¹⁰ and density^{6,26} tests. The glass transition temperature T_g is a material constant available in the literature for numerous polymers.^{2,9} The model could probably be improved by considering the rate dependence of T_g . The quantities such as the modulus of the crystalline phase E_c and the characteristic ratio of macromolecules C_∞ are more difficult to find for every polymer. In this case, as a practical approach, values for the closest known material should be assumed. Here the crystalline modulus of commonly used PA6 was taken as a proxy for PA11. Moreover the model ignores any possible effects of parameters like crystallite size, distribution, and orientation or molecular weight distribution. It should be possible to develop the model further and consider these effects in detail. Predictions should also improve once better input data is available. Nevertheless, the good match between the model and experiment indicates that the approach taken here is sufficiently accurate for Polyamide 11.

The main limitation of the proposed model is its semiempirical nature. Consequently the model cannot provide any theoretical understanding of property emergence from the structure in the microscale. It did, however, bring some insights into the workings in larger scales, e.g. it evaluated the role of crystallites in the plastic deformation and proposed the existence of a mechanical equilibrium. The theory does not account for the modulus strain rate dependence, which corresponds to testing at the arbitrary “standard” rate. Predictions may therefore deviate from experiment in extreme cases, however high accuracy has been obtained in literature for commonly used loading rates.⁹ Moreover the model does not have any theoretical basis to evaluate the effects of plasticizers and it is best applicable to dried specimens. Nevertheless for important polymers, water absorption¹⁹ (acting as plasticizer) and plasticizer extraction² have been linked to changes of the mechanical properties. Therefore, empirical softening factors can be used to estimate the properties of water saturated samples with residual plasticizer content in place. Results for Polyamide 11 suggest that this produces predictions relevant from practical point of view.

CONCLUSIONS

Multiscale modeling results have been compared with experiments for PA11 hydrolysis during water exposure in 120°C. Experiments were shown in the initial article of the series (Part 1). The model was divided into an article describing morphological parameters during degradation (Part 2), as reported previously, and this work treating the mechanical properties (Part 3).

For all tested properties the modeled trend is close to the experimental results. This similarity confirms that the modeling approach chosen here gives relevant results. It also confirms that hydrolysis induced chain scission and chemicrystallization are the two main mechanisms of property change, because these two mechanisms are central to all modeling used. A very good match between model and experiment has been already reported in the case of density and crystallinity evolution. In this work equally good predictions were found for the tensile yield strength, storage modulus and embrittlement threshold.

Results for the tensile strength suggest that the crystalline phase does play a role in plastic deformation as opposed to the view that this is solely a matter of the amorphous phase. The model predicted the existence of mechanical equilibrium between effects of macromolecule degradation and increased degree of crystallinity.

The results suggest that the multiscale modeling methodology can provide faster and less labor extensive alternatives for accelerated aging tests when it comes to long-term property evaluation.

ACKNOWLEDGMENTS

This work is a part of the “PolyLife” project realized between SINTEF Materials and Chemistry, NTNU, PETROBRAS, ROSEN Group, Kongsberg Oil & Gas Technologies, and FMC Technologies. The authors express their gratitude for the financial support by the Research Council of Norway (grant 193167). Randi Berggren performed accelerated aging and mechanical tests as part of her master thesis at NTNU.

REFERENCES

1. API Technical Report 17TR2. The Ageing of PA-11 in Flexible Pipes; API Publishing Services: Washington, DC, **2003**.
2. Rilsan® PA11: Created From a Renewable Source; Arkema: France, **2012**.
3. Teal, J. M.; Howarth, R. W. *Environ. Manage.* **1984**, *8*, 27.
4. Flynn, J. H. *J. Therm. Anal. Calorimetry* **1995**, *44*, 499.
5. Mazan, T.; Jørgensen, J. K.; Echtermeyer, A. T. *J. Appl. Polym. Sci.* **2015**, *132*, 12039.
6. Mazan, T.; Berggren, R.; Jørgensen, J. K.; Echtermeyer, A. T. *J. Appl. Polym. Sci.* **2015**, *132*, 6249.
7. Wu, P.; Siesler, H. W. *Chem. Mater.* **2003**, *15*, 2752.
8. Jacques, B.; Werth, M.; Merdas, I.; Thominette, F.; Verdu, J. *Polymer* **2002**, *43*, 6439.
9. Bicerano, J. Prediction of Polymer Properties; Marcel Dekker AG: New York, **2002**.
10. El-Mazry, C.; Correc, O.; Colin, X. *Polym. Degrad. Stab.* **2012**, *97*, 1049.
11. Flory, P. J. Principles of Polymer Chemistry; Cornell University Press: Ithaca, **1953**.
12. Fermeglia, M.; Prich, S. *Prog Org Coat.* **2007**, *58*, 187.
13. Kremer, K.; Müller-Plathe, F. *Mol. Simul.* **2002**, *28*, 729.
14. Bouvard, J. L.; Ward, D. K. *J. Eng. Mater. Technol.* **2009**, *131*, 041206.
15. van Krevelen, D. W. Properties of Polymers; Elsevier: Amsterdam, **1990**.
16. Halpin, J. C.; Kardos, J. L. *J. Appl. Phys.* **1972**, *43*, 2235.
17. Sakurada, I.; Kaji, K. *J. Polym. Sci. Part C: Polym. Lett.* **1970**, *31*, 57.
18. Flory, P. J.; Williams, A. D. *J. Polym. Sci. Part A-2: Polym. Phys.* **1967**, *5*, 399.
19. Silva, L.; Tognana, S.; Salgueiro, W. *Polym. Test.* **2013**, *32*, 158.
20. Seitz, J. T. *J. Appl. Polym. Sci.* **1993**, *49*, 1331.
21. Fox, T. G.; Loshaek, S. *J. Polym. Sci.* **1955**, *15*, 371.
22. Lennard-Jones, J. E. *Proc. R. Soc. Lond.* **1924**, *106*, 463.
23. Wu, S. *Polym. Eng. Sci.* **1990**, *30*, 753.
24. Kausch, H. H.; Heymans, N.; Plummer, C. J.; Decroly, P. Matériaux polymères: propriétés mécaniques et physiques; Presses Polytechniques et Universitaires Romandes: Lausanne, **2001**.
25. Domingos, E.; Pereira, T. M. C.; Filgueiras, P. R.; Bueno, M. I. M. S.; de Castro, E. V. R.; Guimarães, R. C. L.; de Sena, G. L.; Rocha, W. F. C.; Romão, W. *X-Ray Spectrom.* **2013**, *42*, 79.
26. Karacan, I. *Fibers Polym.* **2005**, *6*, 186.